

# MOLECULAR CONDUCTORS

## Angular Dependent Investigation of the Magnetic Field Induced Superconducting Phase of $\lambda$ -(BETS)<sub>2</sub>FeCl<sub>4</sub>

Balicas, L., NHMFL

Brooks, J.S., NHMFL

Storr, K., NHMFL

Uji, S., NRIM, Tsukuba, Japan

Akutsu, H., Institute for Molecular Science,  
Okazaki, Japan

Kobayashi, H., Institute for Molecular Science,  
Okazaki, Japan

Tokumoto, M., Electrotechnical Laboratory,  
Tsukuba, Japan

$\lambda$ -(BETS)<sub>2</sub>FeCl<sub>4</sub> is an organic conductor which undergoes a dramatic transition to a highly insulating antiferromagnetic state<sup>1</sup> below 8 K. However, a magnetic field of 11 T at low temperatures removes the AF state, and a metallic state is achieved. The appearance of quantum oscillations above 12 T, for the field applied perpendicular to the conducting planes (i.e.,  $B//b$ -axis), indicates the presence of a true metal with a low dimensional Fermi surface. Recently, Uji and co-workers<sup>2</sup> reported that, above 19 T, the system enters a very low resistance state below 1 K when the magnetic field is applied in-plane. Torque magnetometer measurements by the same group<sup>2</sup> gave evidence that this new high field phase, which was followed up to 20 T, is superconducting.

To further explore the high field character of this novel new phase, we investigated the angular dependent magnetoresistance of the title material up to 33 T in the portable dilution refrigerator system at the NHMFL. Some of the results of this study are presented in Fig. 1. Here, the angle of the magnetic field is taken with respect to the  $b$ -axis of the crystal, and the current and voltage were measured along the  $a$ -axis of the crystal. The data were taken by continuous field sweeps where the angle was changed an average of 2 to 3° after each maximum or minimum field was reached. To avoid going into

the highly insulating AF state, the minimum field was kept at about 11 T. As Fig. 1 shows, indeed, for fields aligned close to the in-plane direction, a very low resistance state is stabilized, starting above 19 T. Because of the very low resistance of the sample, and its rapid decrease in the high field regime, the signal-to-noise ratio of this particular measurement did not allow us to confirm that the resistance was actually zero.

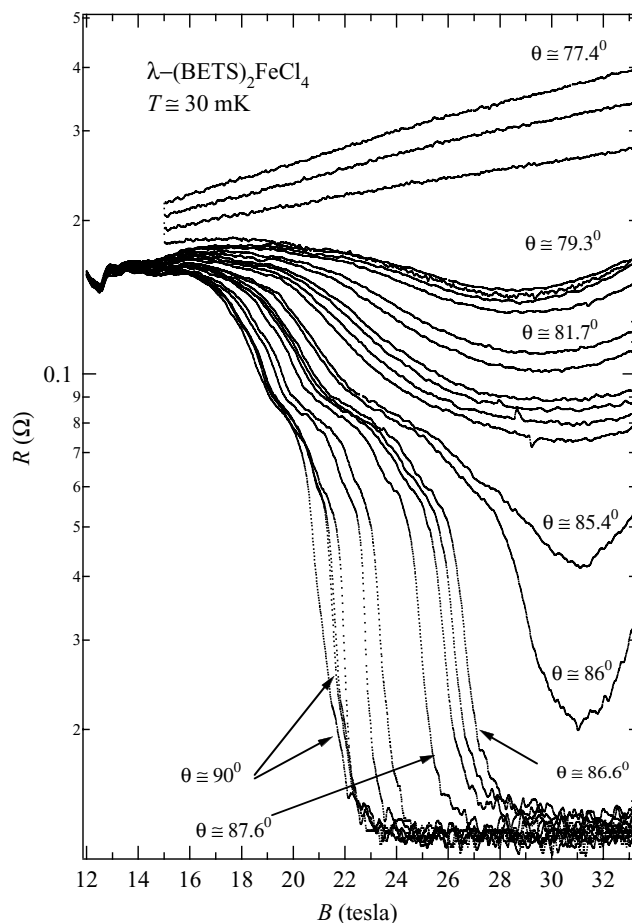


**Figure 1.** Magnetoresistance  $R(\Omega)$  as a function of magnetic field  $B$ , of a  $\lambda$ -(BETS)<sub>2</sub>FeBr<sub>4</sub> single crystal, at  $T=30$  mK, for values of  $\theta$ , which is the angle between  $B$  and  $b^*$  (perpendicular to the conducting planes). (See text for discussion).

There are other remarkable features in the data beyond the stabilization of the new high field state. One is the observation of some anomalous structure around 12 T, and another is the appearance of a shoulder-like structure in the magnetoresistance as the field is further increased. This structure appears at **particular resistance values**, which depend only on the field and its direction. Furthermore, we note that the “superconducting state” persists up to 33 T for the

in-plane field. However, for fields with some out-of-plane component (e.g.  $\theta=86^\circ$ ), the phase seems to be re-entrant towards a normal, metallic state. Based on simple symmetry arguments, the “superconducting state” for perfect in-plane alignment may persist up to, or beyond 40 T.

The title material clearly presents a fundamentally new example of the competition between magnetism and superconductivity in low dimensional systems, and further work is planned to extend these studies to higher DC fields, and also to probe the nature of the “superconducting state.”

**Acknowledgements:** The authors acknowledge support from NSF-DMR 95-10427 and 99-71474 (JSB). One of us (LB) is grateful to the NHMFL for sabbatical leave support. The NHMFL is supported through a cooperative agreement between the State of Florida and the NSF through NSF-DMR-95-27035.

<sup>1</sup> Brossard, L., *et al.*, Eur. Phys. J. B, **1**, 439-452 (1998), and references therein.

<sup>2</sup> Shinagawa, H., *et al.*, Bull. Jap. Phys. Soc., Niigata, Japan, Sept. 22-23, 2000; Uji, S., *et al.*, to be published.

## Shubnikov - de Haas Effect and Yamaji Oscillations in the Antiferromagnetically Ordered Organic Superconductor $\kappa$ -(BETS)<sub>2</sub>FeBr<sub>4</sub>: A Fermiology Study

Balicas, L., NHMFL

Brooks, J.S., NHMFL

Storr, K., NHMFL

Graf, D., NHMFL

Uji, S., NRIM, Tsukuba, Japan

Shinagawa, H., NRIM, Tsukuba, Japan

Terai, Y., NRIM, Tsukuba, Japan

Yakabe, Y., NRIM, Tsukuba, Japan

Terakura, C., NRIM, Tsukuba, Japan

Terashima, T., NRIM, Tsukuba, Japan

Ojima, E., Institute for Molecular Science,  
Okazaki, Japan

Kobayashi, H., Institute for Molecular Science,  
Okazaki, Japan

Fujiwara, H., Institute for Molecular Science,  
Okazaki, Japan

Kobayashi, A., Univ. of Tokyo, Japan

Tokumoto, M., Electrotechnical Laboratory,  
Tsukuba, Japan

The Shubnikov - de Haas effect (SdH) effect and angular dependent magnetoresistance oscillations (AMRO) have been measured<sup>1</sup> in the organic superconductor:<sup>2</sup>  $\kappa$ -(BETS)<sub>2</sub>FeBr<sub>4</sub>. Our AMRO studies provide a clear signature of a closed 2D FS warped along  $k_z$  (the electronic wave vector perpendicular to the FS closed cross-section). In contrast to its isostructural compound,<sup>3</sup>  $\kappa$ -(BETS)<sub>2</sub>FeCl<sub>4</sub>, the SdH oscillations, as shown in Fig. 1 for different field directions with respect to the conducting planes, reveal three Fermi Surface (FS) closed orbits,  $\alpha$ ,  $\beta$ , and  $\gamma$ , whose cross sectional areas are 19.8 %, 99.9 %, and 2.4 % of the first Brillouin zone, respectively. The conduction electron effective masses were found to be:  $\mu_\alpha=(4.7\pm0.2)m_e$ ,  $\mu_\beta=(8.0\pm1.0)m_e$ , and  $\mu_\gamma=(2.0\pm0.2)m_e$ .

The FS derived from our measurements is *not* in agreement with available band structure calculations based on the room temperature crystallographic structure. In particular, the observation of a  $\gamma$

orbit is not expected at all. This discrepancy is not surprising since a structural phase transition is observed below 150 K. Also the original FS may be partially reconstructed by the AF transition observed at 2.5 K, as well as by subsequent magnetic field induced phase transitions among different magnetic states. Although its FS geometry should be quite similar to that of  $\kappa$ -(BETS)<sub>2</sub>FeCl<sub>4</sub>, we observe an important enhancement of the effective mass compared to that obtained for the Cl compound, which may suggest an important interaction between localized Fe<sup>3+</sup> magnetic moments and itinerant  $\pi$  electrons. Indeed,  $\mu_{\beta}$  is among the heaviest masses ever reported for an organic conductor. We note also that, as shown in the inset of Fig. 1, there are features in the magnetoresistance which indicate that transitions

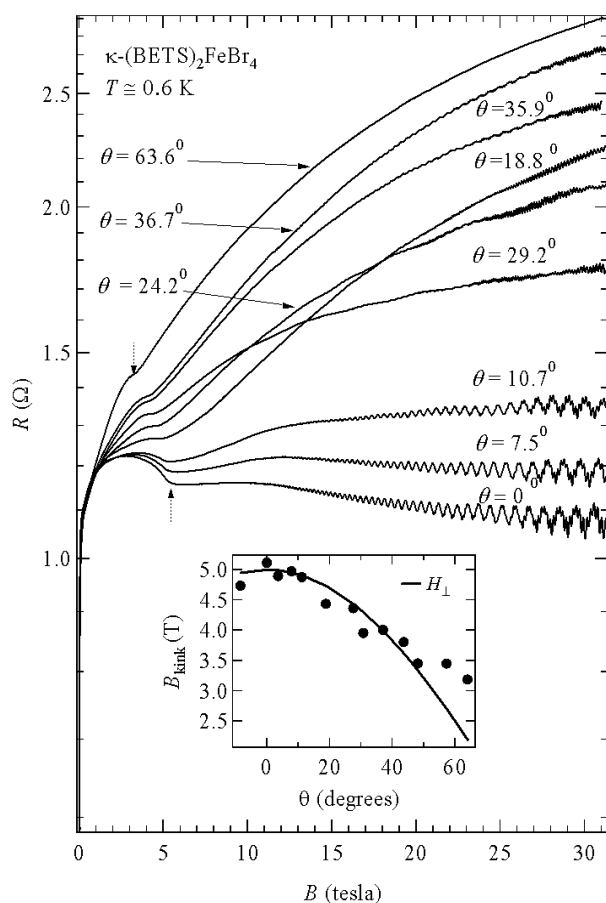


**Figure 1.** Magnetoresistance  $R(\Omega)$  as a function of magnetic field  $B$ , of a  $\kappa$ -(BETS)<sub>2</sub>FeBr<sub>4</sub> single crystal, at  $T \approx 0.6$  K, for several values of  $\theta$  which is the angle between  $B$  and  $b^*$  (perpendicular to the conducting planes). The superconducting state is destroyed by about 0.1 T, after which there is an apparent magnetic transition that depends on magnetic field direction, as shown in the inset.

of a magnetic character occur as a function of tilted magnetic field and temperature. The intriguing proximity of  $T_c$  to  $T_N$  deserves special attention, since this compound could be an ideal candidate to explore the possibility of a superconducting pairing based on spin fluctuations. We suggest that an NMR study, as well as electrical transport experiments, under hydrostatic pressure, in the present compound would be of great interest in order to further explore the interplay between AF and SC.

**Acknowledgements:** The authors acknowledge support from NSF-DMR 95-10427 and 99-71474 (JSB). One of us (LB) is grateful to the NHMFL for sabbatical leave support. The NHMFL is supported through a cooperative agreement between the State of Florida and the NSF through NSF-DMR-95-27035.

- <sup>1</sup> Balicas, L., *et al.*, Solid State Commun., **116**, 557-562 (2000).
- <sup>2</sup> Kobayashi, H., *et al.*, J. Am. Chem. Soc., **118**, 368 (1996); Ojima, E., *et al.*, J. Am. Chem. Soc., **121**, 5581 (1999).
- <sup>3</sup> Tokumoto, M., *et al.*, Synthetic Metals, **86**, 2161 (1997); Brossard, L., *et al.*, Eur. Phys. J. B, **1**, 439 (1998).

## Millimeter-Wave Spectroscopy of the Organic Spin-Peierls System $\beta'$ -(ET)<sub>2</sub>SF<sub>5</sub>CF<sub>2</sub>SO<sub>3</sub> $\blacktriangledown$ IHRP $\blacktriangleleft$

Brooks, J.S., NHMFL/FSU, Physics  
Ward, B.H., NHMFL  
Rutel, I., NHMFL  
Schlueter, J.A., Argonne National Laboratory  
Winter, R.W., Portland State Univ., Chemistry  
Gard, G.L., Portland State Univ., Chemistry

The first purely organic BEDT-TTF spin-Peierls system,<sup>1,2</sup>  $\beta'$ -(ET)<sub>2</sub>SF<sub>5</sub>CF<sub>2</sub>SO<sub>3</sub>, has been confirmed<sup>3</sup> using a high-frequency electron spin resonance (EPR) cavity perturbation technique. The material exhibits the characteristics of a quasi-one-dimensional (1D) Heisenberg antiferromagnetic spin system above 30 K, but undergoes a second-order transition, at  $T_{SP}=33$  K, to a singlet ground state, due to a progressive spin-lattice dimerization. The spin-Peierls state is evidenced by a sharp drop in the spin susceptibility

below 24 K for the magnetic field (of order 2.5 T) parallel to each of the three principle axes (i.e.  $H//a$ ,  $H//b$ , and  $H//c$ ). The spin-Peierls distortion based on  $g$  value shift analysis appears to be predominately along the crystallographic  $b$  axis. The singlet-triplet gap,  $\Delta(0)=114$  ( $\pm 21$ ) K, was determined using a modified BCS theory.

In Fig. 1, we show the crystal structure, and in Fig. 2 we present the experimental results. In Fig. 3 the temperature dependence of the integrated resonance intensity is given, and in Fig. 4 the anisotropic  $g$ -shift is shown. The measurements were performed with the millimeter-wave vector network analyzer (MVNA). This method, which involves a perturbative resonant cavity method is particularly suited for researchers who have interest in precision EPR measurements at magnetic fields and corresponding resonance frequencies higher than conventional X-band measurements. The experimental set-up is sketched in Fig. 5.

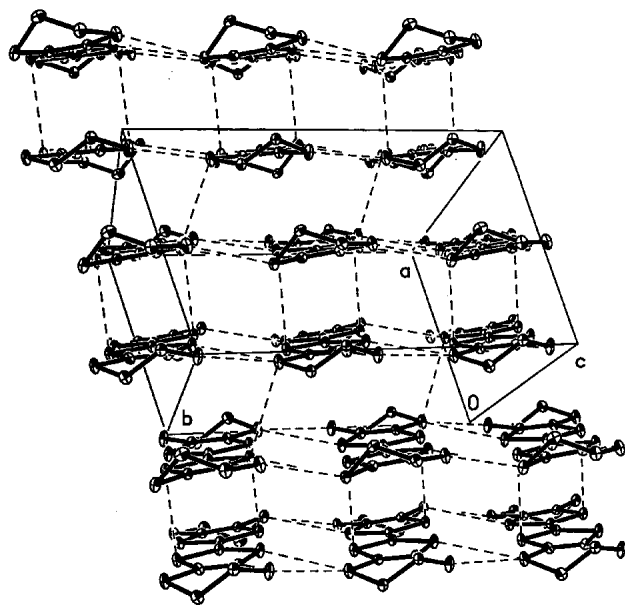


**Figure 1.** View of the ET cation layer in  $\beta'$ -(ET)<sub>2</sub>SF<sub>5</sub>CF<sub>2</sub>SO<sub>3</sub> looking down the long axis of the molecule. The dashed lines indicate S...S van der Waals contacts less than 3.6 Å. The ET molecules are dimerized and form 1D chains predominately along the  $b$  axis.

The behavior shown in Fig. 3, where the spin susceptibility is observed to vanish in all three crystallographic directions, is generally accepted as characteristic of a spin-Peierls transition. We note that in the case of a BCS-like transition, the general rule for the relationship between the critical temperature for  $H=0$  and the critical field for  $T=0$  is approximately  $H_c(T=0)/T_{sp}(H=0)=k_B/\mu_B$  (i.e. the ratio of Boltzmann constant to the Bohr magneton). Hence, based on the low field X-band EPR data, we might expect that  $H_c(T=0)$  would be of order 35 T, and not of order 5 T as the inset of Fig. 3 suggests, and the  $H$ - $T$  phase diagram proposed must be taken as tentative, pending further higher field investigations, which are now in progress.

**Acknowledgements:** The authors acknowledge support from IHRP/NHMFL 5031, NSF-DMR 95-10427 and 99-71474 (JSB). The NHMFL is supported through a cooperative agreement between the State of Florida and the NSF through NSF-DMR-95-27035. Work at Argonne National Laboratory was supported by the U.S. Department of Energy, Office of Basic Energy Sciences, Division of Materials Sciences, under contract No. W-31-109-ENG-38. Work at Portland State University was supported by NSF Grant No. CHE-9904316 and the Petroleum Research Fund ACS-PRF 34624-AC7.

<sup>1</sup> Geiser, U., *et al.*, Am. Chem. Soc., **118**, 9996–9997 (1996).

<sup>2</sup> Ward, B.H., *et al.*, Chem. Mat., **12**, 343-351 (2000).

<sup>3</sup> Ward, B.H., *et al.*, J. Phys. Chem., in press.

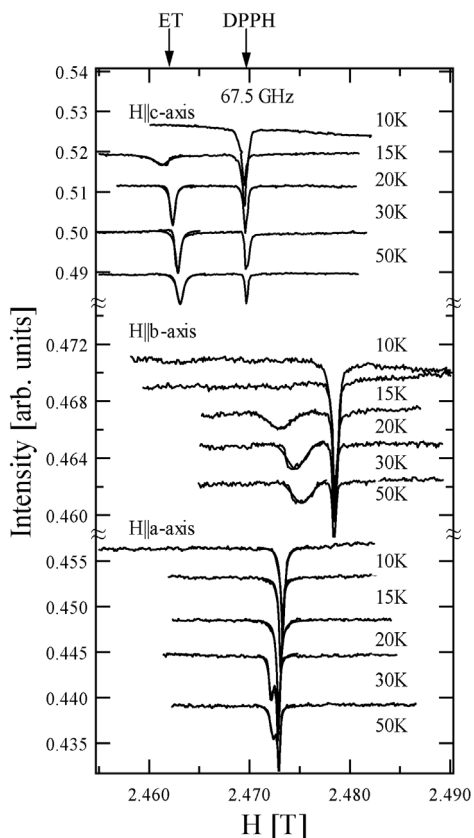


**Figure 2.** Evolution of the EPR signal as the temperature is raised from 10 to 50 K. (Spectra are offset for clarity.) DPPH, included for field calibration, appears as a single resonance up field from the ET resonance. Each spectrum was fit to a Lorentzian line shape.

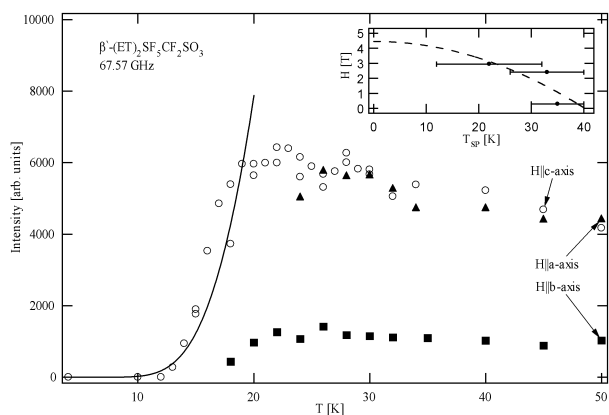


**Figure 3.** The temperature dependence of the EPR integrated absorption for the resonance line at 67.5 GHz for all three orientations ( $H||a$ ,  $H||b$ , and  $H||c$ ). The inset shows the fit (dashed line) below  $T_{sp}$  using the modified BCS fit:  $H_c = H_0[1-(T/T_c)^2]$ .

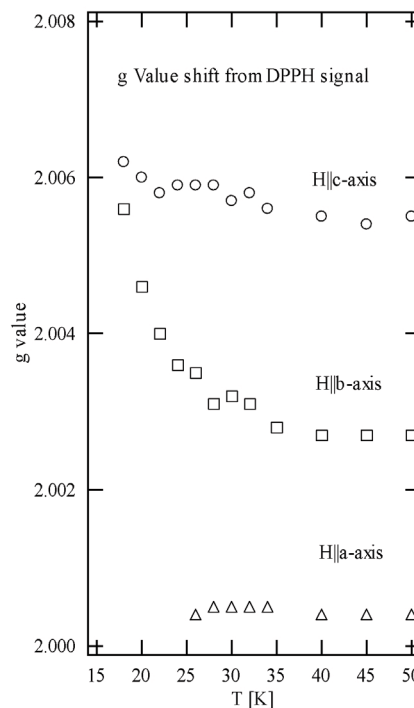


**Figure 4.** The temperature dependence of the  $g$  value for all three orientations. For the  $a$  and  $c$  axis parallel to the external magnetic field the  $g$  value is relatively constant, while for the  $b$  axis parallel to the external magnetic field the  $g$  value increases below  $T_{sp}$ .

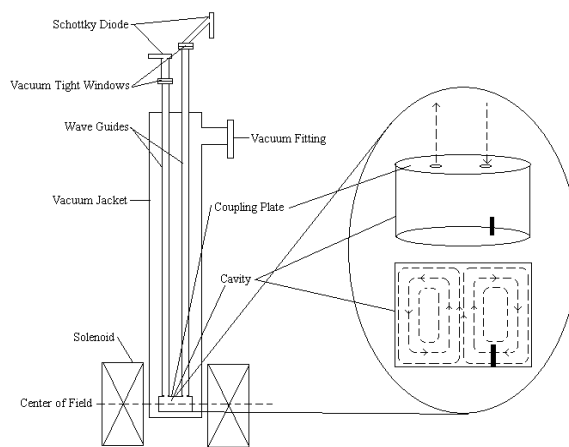


**Figure 5.** A schematic of the experimental setup, including the Schottky diodes, wave guides, coupling plate, cavity, vacuum jacket, and the magnet. The dashed line indicates the center of the magnet. A 3D view of the cavity showing the position of the sample at the bottom of the cavity (upper part). The AC magnetic field ( $H_{AC}$ ) distribution within the cavity for the TE011 mode. The external DC magnetic field ( $H_{DC}$ ) is applied parallel to the cavity axis so that  $H_{AC}$  is perpendicular to  $H_{DC}$  (lower part).



## Anisotropic Critical Field Study of $\alpha\text{-(ET)}_2\text{NH}_4\text{Hg(SCN)}_4$ Using rf Penetration

Coffey, T., Clark Univ., Physics

Agosta, C.C., Clark Univ., Physics

Gao, H., Clark Univ., Physics<sup>1</sup>

Anzai, H., Himeji Institute of Technology

Tokumoto, M., Electrotechnical Laboratory

$\alpha\text{-(ET)}_2\text{NH}_4\text{Hg(SCN)}_4$  ( $\text{ET-NH}_4$ ), is the only superconductor in the  $\alpha\text{-(ET)}_2\text{MHg(SCN)}_4$  ( $\text{M}=\text{K}, \text{NH}_4, \text{Tl}, \text{Rb}$ ) family of organic salts. We have measured critical magnetic field ( $H_{c2}$ ) data of ( $\text{ET-NH}_4$ ) with  $\mathbf{B}$  applied  $\perp$  and  $\parallel$  to the AC plane down to 30 mK in the 18 T superconducting magnet with the top loading dilution refrigerator. We resolved  $H_{c2}$  from rf penetration depth ( $\lambda$ ) measurements using the tunnel diode oscillator technique. Our results are significantly different than two earlier studies<sup>2,3</sup> which had used resistance measurements to resolve  $H_{c2}$ . When  $\mathbf{B}$  is  $\perp$  to the conducting layers, we see evidence for some kind of flux transition below  $H_{c2}$  which changes from first to second order as the temperature increases. The phase diagram in Fig. 1 looks similar to

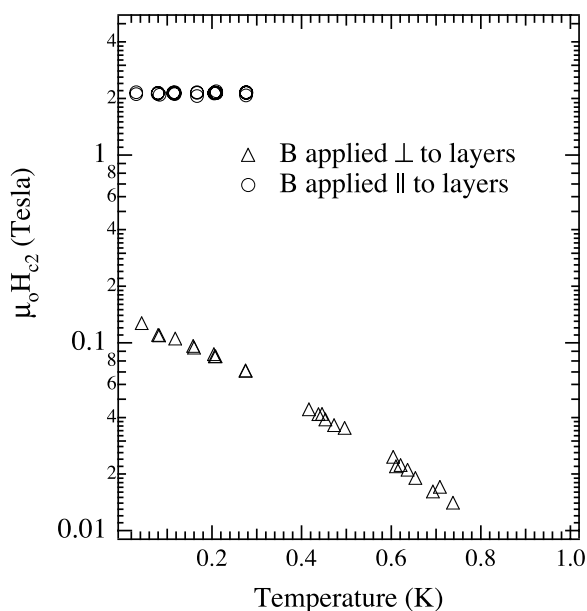


**Figure 1.** The superconducting phase diagram of  $\alpha\text{-(ET)}_2\text{NH}_4\text{Hg(SCN)}_4$ . The higher temperature points where the applied field is  $\perp$  to the layers were measured in our own magnet system at Clark University.

(BEDO-TTF) $_2\text{ReO}_4$  and  $\lambda\text{-(BETS)}_2\text{GaCl}_4$ , suggesting the three systems share a similar unconventional mechanism for superconductivity.<sup>4</sup> When  $\mathbf{B}$  is  $\parallel$  to the most conducting layers,  $H_{c2}$  exceeds the Pauli paramagnetic limit. Our data indicates that  $H_{c2}(\theta)$  at 100 mK has a sharp peak with a rounded top instead of the previously reported cusp-like shape at 800 mK. Our data also shows that  $H_{c2}(T)$  is flat from 30 mK to 300 mK. Below  $H_{c2}/2$ ,  $\lambda$  is strongly hysteretic and shows a greater dependence upon  $d\mathbf{B}/dt$  than temperature.

**Acknowledgements:** We would like to thank Eric Palm and Tim Murphy for providing a great deal of support and facilitating this research.

<sup>1</sup> Current address: Princeton Univ., Electrical Engineering

<sup>2</sup> Shimojo, Y., *et al.*, J. of Superconductivity, **12**, 501,(1999).

<sup>3</sup> Brooks, J.S., *et al.*, Synthetic Metals, **70**, 839 (1995).

<sup>4</sup> Agosta, C.C., *et al.*, Synthetic Metals, **103**, 1795 (1999).

## Proof of Interplane Coherence Using Cyclotron Harmonics in the Organic Superconductor $\beta\text{''-(BEDT-TTF)}_2\text{SF}_5\text{CH}_2\text{CF}_2\text{SO}_3$

Edwards, R.S., Univ. of Oxford, Physics

Symington, J.A., Univ. of Oxford, Physics

Rzepniewski, E., Univ. of Oxford, Physics

Singleton, J., Univ. of Oxford, Physics

Ardavan, A., Univ. of Oxford, Physics

Schlueter, J., Argonne National Laboratory

Many correlated electron systems that are of fundamental or technological interest have very anisotropic electronic bandstructure. Examples include the “high- $T_c$ ” cuprates,<sup>1</sup> layered phases of the manganites<sup>2</sup> and ruthenates,<sup>3</sup> semiconductor superlattices,<sup>4</sup> and crystalline organic metals.<sup>5,6</sup> Such systems are often characterized by a tight-binding Hamiltonian in which the ratio of the interlayer transfer integral to the average intralayer transfer integral is much less than 1. The question arises as to whether these systems possess coherent or incoherent interlayer charge transfer;<sup>1,5-7</sup> i.e., whether or not their Fermi surface (FS) extends in the interlayer direction. Experimental tests for incoherence have thus far

proved inconclusive; e.g., semiclassical models can reproduce angle-dependent magnetoresistance oscillation (AMRO) data equally well when the interlayer transport is coherent or “weakly coherent.”<sup>6,7</sup>

We report cyclotron resonance (CR), along with its second and third harmonics, in the quasi-two-dimensional organic superconductor  $\beta''$ -(BEDT-TTF)<sub>2</sub>SF<sub>5</sub>CH<sub>2</sub>CF<sub>2</sub>SO<sub>3</sub>.<sup>8</sup> The magnetic field orientation dependence of the intensities of the fundamental CR and its harmonics very strongly suggests that the Fermi surface is extended in the interplane direction (i.e., that the interlayer charge transfer is coherent), in contradiction with recent proposals. Fig. 1 shows the magnetic field dependence of the transmission through a resonant cavity loaded with a sample for several values of  $\theta$  ( $\theta$  is the angle between the normal to the Q2D planes and the magnetic field); the cavity can rotate with respect to the applied field (i.e., change the angle  $\theta$ ).<sup>8,9</sup> Data for two values of  $\phi$  are shown ( $\phi$  defines the plane of rotation of the field). The feature at  $\sim 2$  T on all sweeps is a background of the apparatus.<sup>8</sup> At intermediate fields, broad resonances can be seen. For  $105^\circ$ , one resonance moves to higher fields with increasing angle. The position of the resonance in magnetic

field for different angles is consistent with CR.<sup>6,8</sup> At  $\phi=45^\circ$ , another resonance appears for higher  $\theta$  at approximately half the field of the main CR. This resonance is also seen for  $\phi=75^\circ$  and  $15^\circ$ ; it is the second harmonic of the main CR. At some  $\theta, \phi$ , a third harmonic of the CR becomes visible.

Fig. 1(c) shows the cross section of a warped Q2D FS section (warping greatly exaggerated). For a general orientation of the field, quasiparticles follow orbits about the FS such that the  $z$ -component of their real space velocity,  $v_z$ , oscillates. In our measurement geometry, the dissipation caused by the sample is dominated by interplane currents, i.e., by the behavior of  $v_z$ . If  $\theta$  is small, the orbits

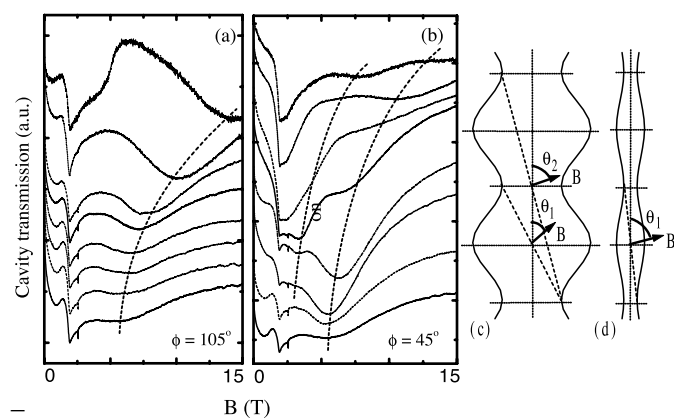


**Figure 1.** (a) Transmission of the resonant cavity loaded with a single crystal of  $\beta''$ -(BEDT-TTF)<sub>2</sub>SF<sub>5</sub>CH<sub>2</sub>CF<sub>2</sub>SO<sub>3</sub> versus magnetic field for  $\theta = 0$  (lowest trace) to  $70^\circ$  (uppermost trace) and  $\phi = 105^\circ$  ( $T = 1.5$  K); the frequency is 70.2 GHz. (b) Equivalent data for  $\phi = 45^\circ$ . (c) and (d) represent two different cross-sections of a warped cylindrical FS; for clarity the warping has been very greatly exaggerated. Cyclotron orbits about the FS are shown schematically as dotted lines for two inclinations of the magnetic field  $B$  to the cylinder axis,  $\theta_1$  and  $\theta_2$ .

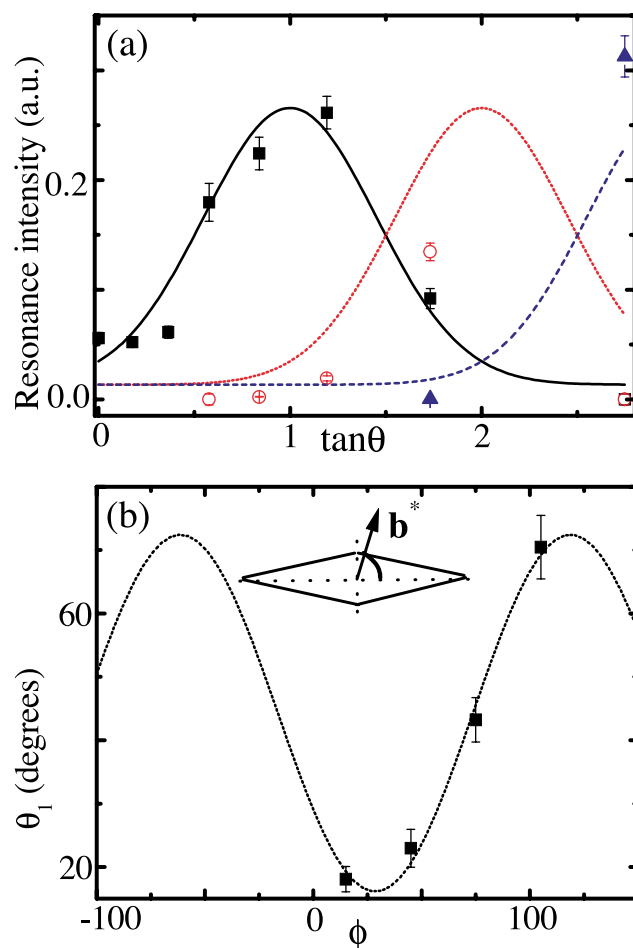


**Figure 2.** (a) Intensity of CRs versus  $\tan\theta$  for  $\phi = 75^\circ$ . Solid curve: predicted intensity of the fundamental CR (data: square points). Dotted curve: predicted intensity of the second harmonic, (data: hollow circles). Dashed curve: predicted intensity of the third harmonic (data: triangles). (b) Predicted  $\theta, \phi$  position of the maximum intensity of the fundamental CR (curve); points are experimental values. Inset: the orientation of the FS cross-section to the crystal's  $b^*$  axis derived from the theory.

remain within the length of one Brillouin zone (BZ) in the  $k_z$ -direction and  $v_z$  oscillates at the cyclotron frequency  $\omega_c$ . As  $\theta$  increases, the orbits extend over several BZs in the  $k_z$ -direction and  $v_z$  acquires oscillatory components at harmonics of  $\omega_c$ . In this way, by assuming an extended Fermi surface in the  $k_z$  direction, the angular behavior of the second and third harmonics can be predicted (Fig. 2a), as can the value of  $\theta, \phi$  at which the maximum amplitude of a particular harmonic occurs (Fig. 2b).<sup>8</sup>

<sup>1</sup> Ioffe, L.B., *et al.*, Science, **285**, 1241 (2000).

<sup>2</sup> Rao, C.N.R., J. Mater. Chem., **9**, 1 (1999).

<sup>3</sup> Bergemann C., *et al.*, Phys. Rev. Lett., **84**, 2662 (2000).

<sup>4</sup> Kelly, M.J., Low Dimensional Semiconductors (Oxford University Press 1995).

<sup>5</sup> Strong, S.P., *et al.*, Phys. Rev. Lett., **73**, 1007 (1994).

<sup>6</sup> Singleton, J., Reports on Progress in Physics, **63**, 1111 (2000).

<sup>7</sup> McKenzie, R.H., *et al.*, Phys. Rev. Lett., **81**, 4492 (1998).

<sup>8</sup> Schrama, J.M., *et al.*, J. Phys.: Condens. Matter, **9**, 2235 (2001)

## High Field Calorimetry of Organic Conductors in the Portable Dilution Refrigerator

Fortune, N., Smith College, Physics  
Peabody, L., Smith College

In quasi-1D and quasi-2D organic conductors, some of the most interesting phases and phase transitions occur at the extremes of high magnetic fields and low temperatures. Calorimetry is one of the most fundamental techniques imaginable for exploring these novel states of matter. To pursue this research, we have developed a new method of reliably producing miniature thermal sensors,<sup>1</sup> a new “spark-bonding” method of attaching thin electrical wires to these sensors without the use of high specific heat solders and epoxies, a new design for miniature, rotatable vacuum chambers with electrical and thermal feedthroughs, and a new and significantly more accurate method of calibrating thermal sensors in high magnetic fields at dilution refrigerator temperatures.<sup>2</sup>

Our previous versions of these miniature vacuum chambers and calorimeters required direct temperature regulation of the  $^3\text{He}$ - $^4\text{He}$  mixture. This apparatus has been used to perform specific heat and magnetothermal measurements<sup>3</sup> of  $\alpha$ -(BEDT-TTF)<sub>2</sub>KHg(SCN)<sub>2</sub> in NHMFL’s 33 T resistive magnet and top-loading portable dilution refrigerator (PDR). In experiments this year (2000), we have tested modifications to these designs that: (1) allow the temperature inside the chamber to be varied independently of the mixture temperature, and (2) replace the metal housing with non-conductive epoxies (while retaining an indium o-ring seal). We have also successfully tested the extension of our calibration method from 18 T to 33 T at temperatures down to 0.1 K.

Many heat capacity measurements require temperature sweeps that begin at temperatures below that available in  $^3\text{He}$  cryostats, but extend above the PDR’s 0.6 K upper temperature limit. The epoxy chamber with variable temperature stage that we tested this year in the PDR now allows measurements between 0.1 K and 4 K up to 33 T. Low frequency field modulation can now be added without inducing significant eddy current heating beyond the previous limits of 0.3 K and 30 T. We have discovered, however, that replacement of the metal housings with epoxy has reduced the shielding of newly-prominent magnet-power-supply-induced noise between roughly 22 and 24 T (and also at selected lower field ranges). Since some of the magnetic-field-induced phase transitions in the quasi-low-dimensional organic conductors, that we are currently studying, occur in this field range, we have chosen to defer discussion of preliminary measurements until we can perform new measurements with improved shielding.

<sup>1</sup> Fortune, N.A., *et al.*, Review of Scientific Instruments, **69**, 133-138 (1998).

<sup>2</sup> Fortune, N.A., *et al.*, Review of Scientific Instruments, **71**, 3825-3830 (2000).

<sup>3</sup> Fortune, N.A., *et al.*, Synthetic Metals, **103**, 2078-2079 (1999).



## Persistent Currents in an Organic Metal “Only” in Strong Magnetic Fields

Harrison, N., NHMFL/LANL

Mielke, C.H., NHMFL/LANL

Balicas, L., NHMFL and Venezuelan Institute for Scientific Research

Brooks, J.S., NHMFL/FSU

Tokumoto, M., Electro-Technical Institute, Japan

The organic metal  $\alpha$ -(BEDT-TTF)<sub>2</sub>KHg(SCN)<sub>4</sub>, along with its sister compounds, is undoubtedly one of the most exotic charge-density wave systems ever to be discovered and one of the materials most strongly suited to research in high magnetic fields. The transition temperature ( $T_p$  to 8 K) is exceptionally low, implying that it is especially vulnerable to magnetic fields. In laboratory accessible fields of 23 T, this material surpasses its Pauli paramagnetic limit, transforming into quite a different phase that is only stable in very strong magnetic fields. See Fig. 1 for a notional phase diagram for this material.

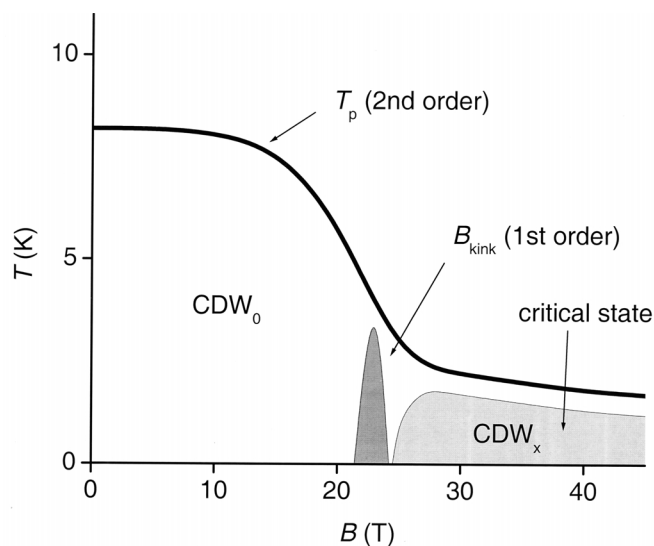


**Figure 1.** Notional phase diagram of  $\alpha$ -(BEDT-TTF)<sub>2</sub>KHg(SCN)<sub>4</sub>.

Recently, a number of experiments have been performed indicating that the high magnetic field CDW<sub>x</sub> phase of  $\alpha$ -(BEDT-TTF)<sub>2</sub>KHg(SCN)<sub>4</sub> closely resembles a superconductor that is not 100% transformed. Notably, AC susceptibility measurements reveal a strong diamagnetic response

at high magnetic fields, particularly at integral Landau level filling factors (by integral filling factors we refer to the magnetic field at which an integral number of Landau levels of the 2D pocket giving rise to the quantum oscillations are filled).<sup>1</sup> An example of such a measurement is shown in Fig. 2a. The presence of an imaginary AC susceptibility component that exceeds the real component implies that we are dealing with currents, similar to those previously observed in pulsed magnetic fields.<sup>2</sup>

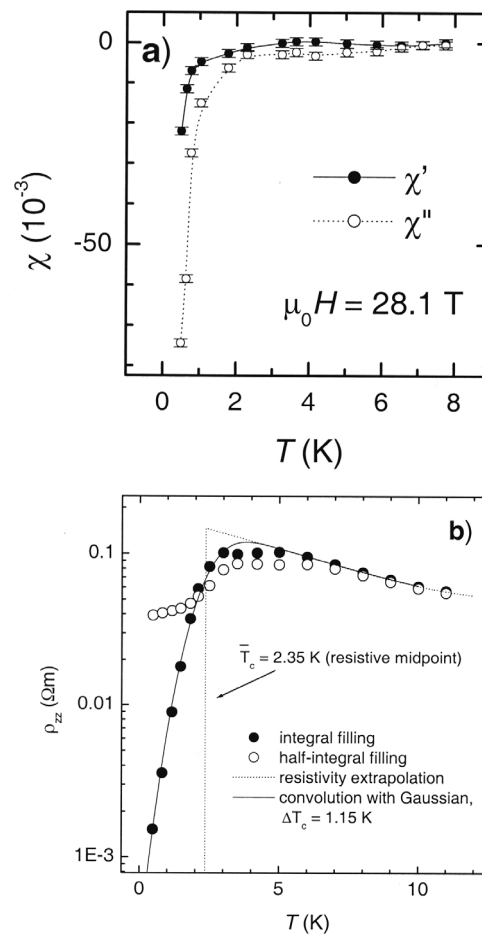


**Figure 2.** (a) AC susceptibility at ~30 T. (b) Temperature dependence of the interlayer resistivity at ~30 T.

Perhaps the most remarkable behavior is presented in Fig. 3a, evidencing the existence of a critical state.<sup>3</sup> By “critical state” we mean that this material exhibits a diamagnetic hysteresis very similar to that of a type II superconductor. This becomes more clear in Fig. 3b where we have subtracted the background.

magnetization as well as the de Haas-van Alphen oscillations, obtained by averaging full rising and falling magnetic field sweeps. The magnetization falls on increasing the field until the current flowing within the sample saturates at a critical value (*i.e.* the critical current  $j_c$ ). On reversing the direction of sweep of the magnetic field, the sample behaves diamagnetically (*i.e.*  $dM/dH < 0$ ), which implies the existence of screening currents within at least  $\sim 1\%$  of the sample. On decreasing the field further, the current eventually saturates once again but this time having a positive magnetization owing to trapped flux within the sample. Experiments performed in a constant field over several tens of minutes show that these currents relax logarithmically as they do in type II superconductors.<sup>3</sup>

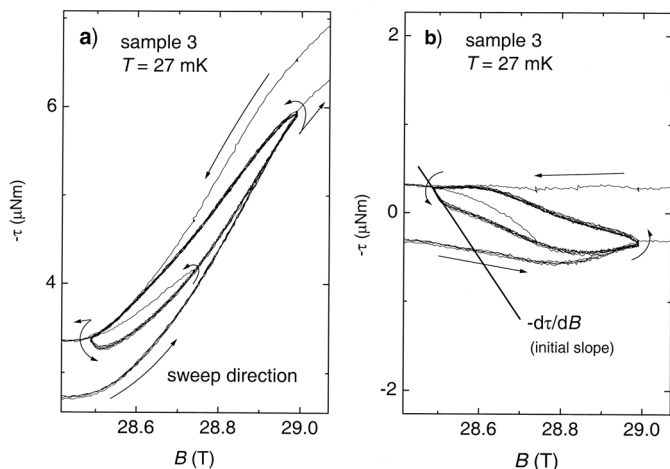


**Figure 3.** Diamagnetic hysteresis measured in the magnetic torque as measured (a) and (b) with the background subtracted.

The near superconducting-like properties of  $\alpha$ -(BEDT-TTF)<sub>2</sub>KHg(SCN)<sub>4</sub> are also reflected in transport measurements. Although there are some 4 to 5 orders of magnitude difference between the intralayer (determined from skin depth measurements) and interlayer (measured directly) resistivities, they behave very similarly; see Fig. 2b. The resistivity is weakly temperature dependent above  $\sim 3$  K, but then drops dramatically below  $\sim 2$  K, particularly at integral filling factors, by approximately two orders of magnitude.<sup>3</sup> The temperature dependence behaves exactly like a transition into a zero resistivity state that is broadened by inhomogeneities (*i.e.* a sharp transition that is convoluted with a Gaussian), as is found to be

the case in many inhomogeneous superconducting systems.<sup>4</sup>

<sup>1</sup> Harrison N., *et al.*, Phys. Rev. Lett. (in press 2001).

<sup>2</sup> Harrison N., *et al.*, Phys. Rev. Lett. **77**, 1576 (1996).

<sup>3</sup> Harrison N., *et al.*, Phys. Rev. **B 62**, 14212 (2000).

<sup>4</sup> Harrison N., to be published.

## To Be or Not to Be Spin-Split

Harrison, N., NHMFL/LANL

Biskup, N., NHMFL

Brooks, J.S., NHMFL/FSU, Physics

Tokumoto, M., Electro-Technical Institute, Japan

A number of published papers have shown that the charge-transfer salt  $\alpha$ -(BEDT-TTF)<sub>2</sub>KHg(SCN)<sub>4</sub>, along with sister compounds, has a complex phase diagram as a function of temperature and magnetic field. Much of this phase diagram is accessible to quantum oscillation experiments such as the de Haas-van Alphen (dHvA) effect. One particularly dramatic first order phase transition takes place in this material at  $B_{\text{kink}} \sim 23$  T. Below this transition, it is thought to be in a commensurate CDW<sub>0</sub> phase, with the dHvA oscillations exhibiting a pronounced second harmonic. Many have attributed this to spin-splitting of the Landau levels in a magnetic field, which then goes away at fields above  $B_{\text{kink}}$ .<sup>1</sup> An alternative model for the split waveform has been proposed but has never been tested.<sup>2</sup>

In order to investigate the true origin of the splitting of the waveform in this material, we measured the magnetic field orientation dependence of the magnetic torque at a variety of magnetic fields both above and below  $B_{\text{kink}}$ . Undoubtedly, the most interesting aspect of these results is that the angle at which the fundamental oscillation frequency experiences a node is exactly the same both above and below  $B_{\text{kink}}$ , suggesting that the product of the effective mass enhancement  $m^*$  with the electron  $g$ -factor  $g$  is insensitive to the phase transition.

An example of the field orientation dependence of the oscillation phase is shown in Fig. 1., together with the functional form of  $\sin\theta\cos S$  (where  $S = \pi m^* g /$

$2\cos\theta$ ) best able to reproduce the correct phase (solid line). For this solid line,  $m^*g \sim 3.67$ . When we insert the value of  $m^*g \sim 4.7$  (as published by Sasaki and Fukase<sup>3</sup>) into  $\sin\theta\cos S$ , however (dotted line), the first node cannot be reproduced. This implies that the value of  $m^*g \sim 4.7$  published by Sasaki and Fukase is most definitely wrong.<sup>3</sup> A detailed analysis of the field orientation dependence of the waveform shows that the frequency doubling effect is the appropriate model.<sup>2</sup>

<sup>1</sup> Harrison N., *et al.*, cond-mat/0011478.

<sup>2</sup> Harrison N., *et al.*, Phys. Rev. Lett., **83**, 1395 (1999).

<sup>3</sup> Sasaki, T., *et al.*, Phys. Rev. B, **62**, 14212 (2000).

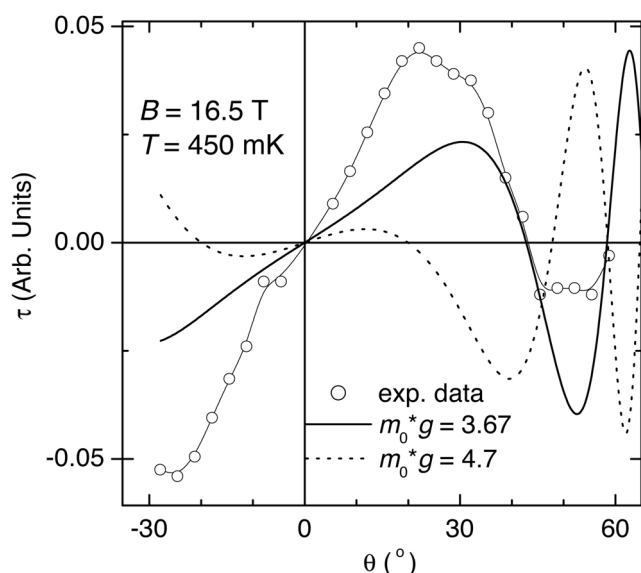


**Figure 1.** Field orientation dependence of the fundamental oscillation amplitude within the CDW<sub>0</sub> phase of  $\alpha$ -(BEDT-TTF)<sub>2</sub>KHg(SCN)<sub>4</sub>. The solid line represents the phase of the oscillations to be expected when  $m^*g \sim 3.67$  while the dotted line represents that expected for  $m^*g \sim 4.7$  (Sasaki and Fukase).

## Pressure Dependence of the Quantum Hall Effect of (TMTSF)<sub>2</sub>ReO<sub>4</sub>

Kang, H., Ewha Womans Univ., Korea, Physics  
Jo, Y.J., Ewha Womans Univ., Korea, Physics  
Kang, W., Ewha Womans Univ., Korea, Physics

Quantum Hall effects are readily observed in the quasi-one-dimensional organic conductors such as (TMTSF)<sub>2</sub>ClO<sub>4</sub>,<sup>1</sup> (TMTSF)<sub>2</sub>PF<sub>6</sub>,<sup>2</sup> and (TMTSF)<sub>2</sub>ReO<sub>4</sub>.<sup>3</sup> However, contrary to the conventional QHE in

semiconductors, unusual features such as Hall sign reversal,<sup>4</sup> missing quantum indices, etc., are commonly observed in organic conductors. Even in (TMTSF)<sub>2</sub>PF<sub>6</sub>, which is believed to be the simplest in the series, Hall sign reversal has been observed over a certain pressure range. Although the standard model of quantized nesting theory<sup>5</sup> has offered a firm basis for the QHE, there is no consistent understanding for these additional features. (TMTSF)<sub>2</sub>ReO<sub>4</sub> is the least studied probably because of its highest critical pressure necessary to stabilize the metallic state at low temperature.

We have performed the Hall resistance measurement of (TMTSF)<sub>2</sub>ReO<sub>4</sub> under various hydrostatic pressures. Several new features drew our attention in the present study. First, in addition to the previously known negative Hall step around 15 T, at least two more new negative indexed quantized states have been observed. Interestingly enough, the negatively indexed states seem to form their own quantum Hall sequence independently from the positively indexed states at high field. Second, low field negatively indexed states are better developed at low pressure while the positively indexed states favor high pressure. When the field is normalized, only the transition fields for low field

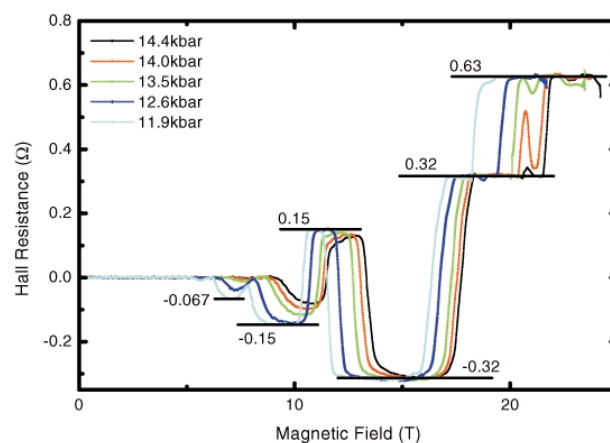


**Figure 1.** The pressure dependence of Hall resistance at around 200 mK. All the values of pressure were measured at room temperature by manganin resistance inside the cell, and the real pressure at low temperature was lower than that by 2 kbar. The Hall resistance data for  $N = 0$  were intentionally removed for clarity.

states could be scaled, to which the standard model can be applied. Third, an isolated Hall resistance peak appears for the narrow pressure interval around 14 kbar.

Most of these experimental findings cannot be explained with the quantized nesting model. We believe that a superlattice potential due to anion ordering plays an important role. Further analysis in consideration of possible mixed anion ordering and in comparison with other compounds will be reported elsewhere.

<sup>1</sup> Ribault, M., *Mol. Cryst. Liq. Cryst.*, **119**, 91 (1985).

<sup>2</sup> Cooper, J. R., *et al.*, *Phys. Rev. Lett.*, **63**, 1984 (1989).

<sup>3</sup> Kang, W., *et al.*, *Phys. Rev. B*, **43**, 11467 (1991).

<sup>4</sup> Balicas, L., *et al.*, *Phys. Rev. Lett.*, **75**, 2000 (1995).

<sup>5</sup> Gor'kov, L. P., *et al.*, *J. Phys. Lett.*, **45**, L433 (1984).

## The Role of Molecular $g$ Anisotropy in Determining EPR Linewidth in Radical-Ion Salts of Me(2,5-Dimethyldicyanoquinonediimine)<sub>2</sub> Class ▀IHRP▴

Krzystek, J., NHMFL

Sienkiewicz, A., Institute of Physics, Polish

Academy of Sciences

Weber, R.T., Bruker Instruments Inc., Billerica, MA

Brunel, L.-C., NHMFL

von Schütz, J.U., Univ. of Stuttgart, Germany,

Physics Institute

Radical ion salts of the series Me(2,5-DMDCNQI)<sub>2</sub>, where Me=Li<sup>+</sup>, ..., Ag<sup>+</sup>; 2,5-DMDCNQI=2,5-dimethyldicyanoquinonediimine, have attracted considerable attention in recent years due to their fascinating electrical and magnetic properties. These properties strongly depend on the metal ion involved, with the Cu<sup>+</sup> salt displaying very high conductivity in a broad temperature range.<sup>1</sup>

The Li<sup>+</sup> salt described in this report has been extensively researched by conventional EPR and non-resonant methods that concentrated on the relationship of magnetic and electrical properties of this compound.<sup>2</sup> HFEPR added a new dimension to this research, namely operating frequency. One of the

most striking observations in HFEPR spectra is the quasi-linear dependence of the single  $g \approx 2$  linewidth on the frequency. This phenomenon does not agree with existing theories<sup>3,4</sup> that predict a constant linewidth above a certain threshold determined by the relationship of spin exchange frequency, and EPR operating frequency. We have thus concentrated on the presence of low-temperature signals detectable below about 35 K as sidebands to the central  $g \approx 2$  line.<sup>5</sup> By following the angular dependence of those sidebands in a single crystal (Fig. 1) at different frequencies, we were able to determine that their splitting scales with frequency. Therefore, we postulate that their origin lies in the molecular  $g$  anisotropy of the 2,5-DMDCNQI anion. This anisotropy is most probably responsible for the quasi-linear dependence of the central  $g \approx 2$  line width on frequency/field in the high temperature regime, where the individual sidebands are washed out by rapid spin exchange. This observation may have a more general significance since similar unexplained phenomena have been observed in other strongly exchanging systems.<sup>6</sup>

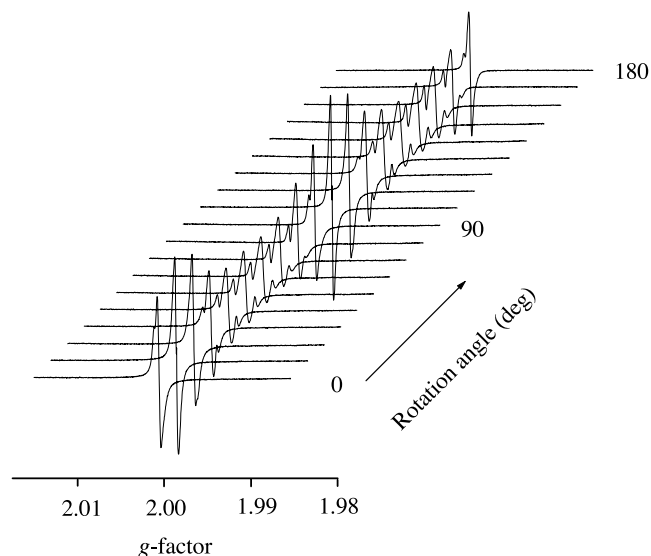


**Figure 1.** Angular dependence of the EPR signal of a Li(2,5-DMDCNQI)<sub>2</sub> single crystal at  $\nu \approx 94.2$  GHz and  $T = 10$  K. The crystal was rotated about its needle axis.

<sup>1</sup> Mori, T., *et al.*, *Phys. Rev. B*, **38**, 5913 (1988).

<sup>2</sup> Krebs, M., Ph.D. thesis, Univ. of Stuttgart, (1995).

<sup>3</sup> Anderson, P.W., *et al.*, *Rev. Mod. Phys.*, **25**, 269 (1953).

<sup>4</sup> Kubo, R., *et al.*, *J. Phys. Soc. Jpn.*, **9**, 888 (1954).

<sup>5</sup> Krzystek, J., *et al.*, 1999 NHMFL Annual Research Review.

<sup>6</sup> Krzystek, J., *et al.*, *J. Magn. Reson.*, **125**, 207 (1997).



# Quantum Melting of the Quasi-Two-Dimensional Vortex Lattice in $\kappa$ -(ET)<sub>2</sub>Cu(NCS)<sub>2</sub>

Mola, M., Montana State Univ., Physics  
 Hill, S., MSU, Physics  
 Brooks, J.S., NHMFL/FSU, Physics  
 Qualls, J.S., Wake Forest Univ., Physics

With the advent of high temperature and organic superconductors, investigations into the mixed state of type-II materials has undergone a renaissance.<sup>1</sup> In particular the thermodynamics and associated phase transitions within the vortex state have drawn considerable interest. Due to extreme purity and lack of metallurgical defects, along with a low  $T_c$  (~10 K) and  $H_{c2}$  (5 T and 30 T with the field applied  $\perp$  and  $\parallel$  to the superconducting layers, respectively), the  $\kappa$ -(ET)<sub>2</sub>Cu(NCS)<sub>2</sub> organic superconductor provides an ideal system for studying the quasi-two-dimensional (Q2D) vortex system over the entire mixed state.

High quality single crystals were mounted on a capacitive cantilever beam torque magnetometer which, in turn, was attached to a single axis rotator allowing for angle dependent measurements.  $\theta=0^\circ$  corresponds to the field parallel to the least conducting  $a$ -axis, while  $\theta=90^\circ$  corresponds to the field parallel to the highly conducting  $bc$ -planes. The entire apparatus was loaded into a  $^3\text{He}/^4\text{He}$  dilution refrigerator situated within the bore of a 20 T superconducting magnet in the millikelvin facility at the NHMFL in Tallahassee, allowing for measurements at temperatures between 25 and 200 mK.

Magnetothermal instabilities in the form of flux jumps were observed at all measurement angles and at temperatures between 25–150 mK. Upon closer inspection of the high field tails of each magnetization sweep at 25 mK we find that, at low angles (Fig. 1a), the amplitudes of the flux jumps decay to zero just before reaching an angle dependent kink in the magnetization. At larger angles (Fig. 1b), the flux jump amplitude is much larger than the amplitude of the kink, making observation of the kink impossible;

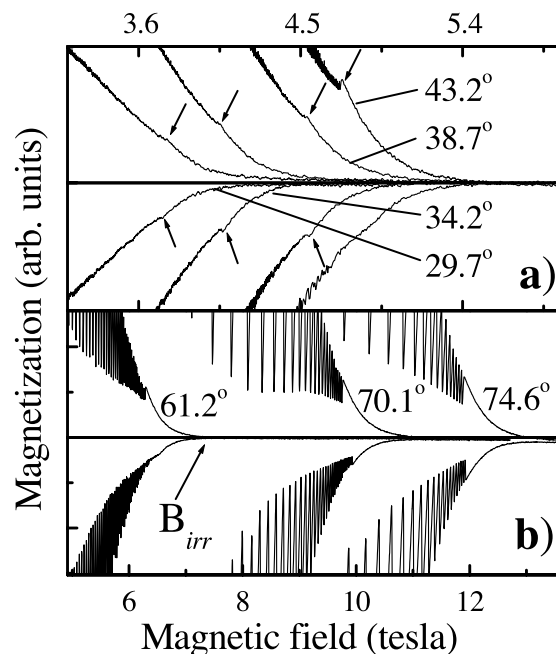


**Figure 1.** Hysteretic magnetization sweeps showing flux jumps. Note the kink in (a), and the abrupt flux jump cessation in (b).

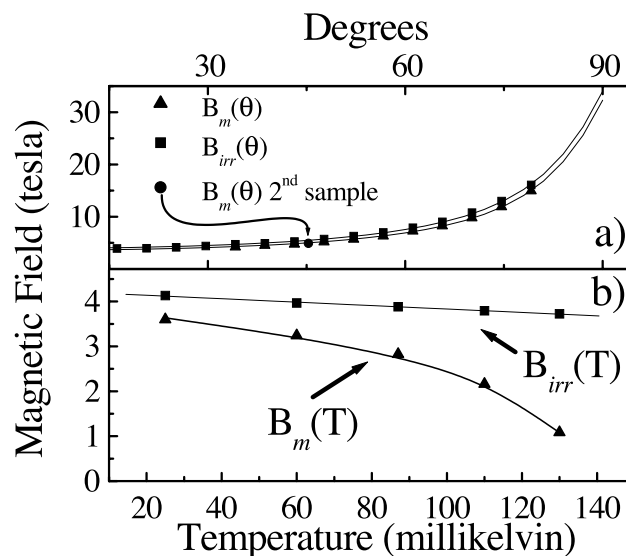


**Figure 2.** Angle and temperature dependence of the melting transition.

however, the flux jumps cease very abruptly at an angle dependent field that merges with the angle dependence of the kink field. We attribute both of these phenomena to a melting of the Q2D vortex lattice.<sup>2</sup> Fig. 2a shows the angle dependence of both the melting field and the irreversibility field with the smooth lines given by fits using the 2D Ginzburg-Landau theory.<sup>3</sup> In Fig. 2b, we plot the temperature



dependence of the melting transition, measured at an angle of  $47^\circ$  and scaled back to  $\theta=0^\circ$  using the above angle dependence. We believe that the negative curvature in the temperature dependence is due to a crossover from a quantum melting to a thermally induced melting transition, as described previously for 2D thin films by Blatter *et al.*<sup>2,4</sup>

**Acknowledgements:** This work was supported by NSF DMR 0071953 and by the Office of Naval Research (N00014-98-1-0538).

<sup>1</sup> Blatter, G., *et al.*, Rev. Mod. Phys., **66**, 1125 (1995).

<sup>2</sup> Mola, M., *et al.*, cond-mat/0008262.

<sup>3</sup> Zuo, F., *et al.*, Phys. Rev. B, **61**, 750 (2000).

<sup>4</sup> Blatter, G., *et al.*, Phys. Rev. B, **50**, 13013 (1994).

## Detailed Modeling of Angle-Dependent Magnetoresistance Oscillations and Fermi-Surface Traversal Resonances

Nam, M.-S., Univ. of Oxford, Physics  
Symington, J.A., Univ. of Oxford, Physics  
Ardavan, A., Univ. of Oxford, Physics  
Singleton, J., Univ. of Oxford, Physics  
Kurmoo, M., IPCMS, Strasbourg, France  
Day, P., The Royal Institution, London

We have developed techniques for extracting more detailed information from angle-dependent magnetoresistance oscillations (AMROs). AMROs occur when a sample's resistance is measured as a function of orientation within a static magnetic field;<sup>1</sup> their high-frequency analogues are Fermi-surface traversal resonances (FTRs). In this summary, we mention two of the new techniques; the data used were recorded at the NHMFL in Tallahassee.

Among the great variety of ground states exhibited by metals based on the molecule BEDT-TTF, those found in  $\alpha$ -(BEDT-TTF)<sub>2</sub>KHg(SCN)<sub>4</sub> have generated particular interest.<sup>1,2</sup> This material was generally believed to form a spin-density-wave at temperatures below about 8 K and magnetic fields below 23 T, but recent work suggests that the ground state is more akin to a charge-density wave.<sup>1,2</sup> It is known that in the low-temperature low-magnetic-

field state, the periodicity of the density-wave causes a reconstruction of the Fermi surface into highly warped quasi-one-dimensional (Q1D) sheets and small quasi-two-dimensional (Q2D) pockets.<sup>2</sup> Using a Boltzmann-transport approach combined with an equivalent circuit model that allows contributions from different parts of the Fermi surface to be combined, we have simulated the AMROs. The Fermi-surface topology used is based on that given in Ref. 2, which seems best able to account for these and other experimental data. Comparisons between model and data give the exact orientation of the nesting vector of the density-wave, and further constrain the ellipticity of the Q2D pockets. The

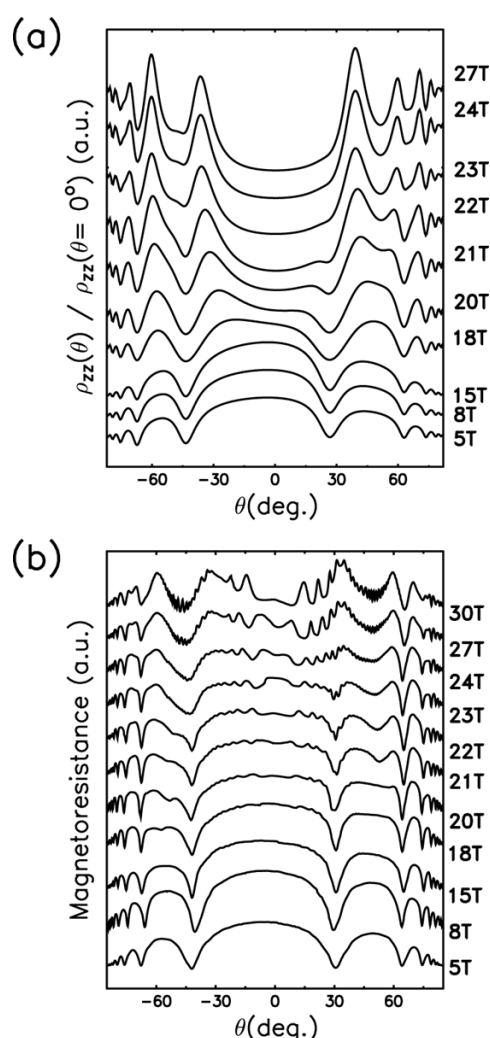


**Figure 1.** Comparison of simulated (a) and experimental (b) AMRO in  $\alpha$ -(BEDT-TTF)<sub>2</sub>KHg(SCN)<sub>4</sub> as a function of field.

simulation is also able to account for the field-dependence of the FTR line width in this material and for the evolution of the AMROs and FTRs with increasing field. A typical simulation and the equivalent experimental data are shown in Fig. 1.

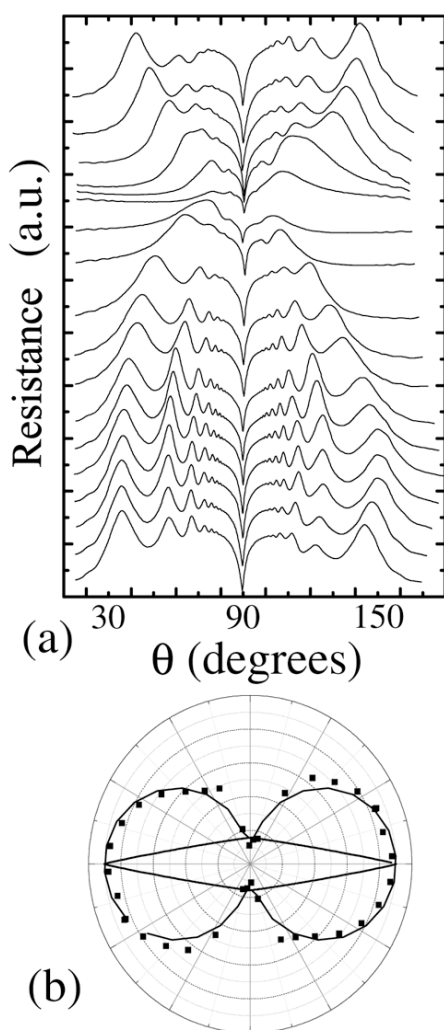


**Figure 2.** (a) AMRO data for  $\beta''$ -(BEDT-TTF) $_2$ SF $_5$ CH $_2$ CF $_2$ SO $_3$  at 10 T and 1.5 K for  $\phi$ -angles  $7\pm 1^\circ$  (top trace)  $17\pm 1^\circ$ ,  $27\pm 1^\circ$ , ...,  $177\pm 1^\circ$  (bottom trace).  $\phi=0$  corresponds to rotation in the  $\mathbf{a}^*\mathbf{c}^*$  plane of the crystal to within the accuracy of the infrared orientation. (b) The  $\phi$  dependence of  $k_{\parallel}$  from the periodicity of the AMRO in Fig. 2(a) (points); the “figure of eight” solid curve is a fit. The resulting fitted Fermi-surface pocket (elongated diamond shape;  $j=1.1$ ) is shown within.

A second example of the new techniques is shown in Fig. 2, which displays AMROs in the superconductor  $\beta''$ -(BEDT-TTF) $_2$ SF $_5$ CH $_2$ CF $_2$ SO $_3$ .<sup>3</sup> The sample's angular coordinates are the angle  $\theta$  between the magnetic field  $\mathbf{B}$  and  $\mathbf{c}^*$ , and the angle  $\phi$  defining the plane of rotation.<sup>1</sup> The AMRO

maxima occur at angles  $\theta_n$  given by  $c'k_{\parallel}\tan\theta_n=\pi(n\pm 1/4...)+f(\Phi)$ , where  $c'$  is the effective interplane spacing,  $k_{\parallel}$  is the maximum Fermi wave-vector in the plane of rotation,  $n$  is an integer, and  $f(\phi)$  is a function of the plane of rotation of the field.<sup>1</sup> The + and – signs correspond to  $\theta_n > 90^\circ$  or  $\theta_n < 90^\circ$  respectively. The AMRO data are most accurately fitted by a non-elliptical Fermi surface cross section,  $(k_x/a)^j + (k_y/b)^j = 1$ . A free-parameter fit yielded  $j=1.1\pm 0.1$  and a ratio  $a/b=9.0\pm 0.1$ , leading to the “diamond-shaped” Fermi surface shown in Fig. 2b; the Fermi surface long axis makes an angle of  $68\pm 3^\circ$  with the  $\mathbf{b}^*$  axis of the crystal. The fitted Fermi-surface cross-section has an area corresponding to a de Haas-van Alphen frequency of  $F=196\pm 3$  T, in excellent agreement with quantum-oscillation studies. The disagreement between the area deduced from AMRO and the quantum oscillation experiments was significantly worse if the cross-section was constrained to be elliptical ( $j=2$ ).<sup>3</sup>

<sup>1</sup> For a recent review see Singleton, J., Reports on Progress in Physics, **63**, 1111 (2000).

<sup>2</sup> Harrison, N., *et al.*, J. Phys.: Condens. Matter, **11**, 7227 (1999).

<sup>3</sup> Nam, M.-S., *et al.*, J. Phys.: Condens. Matter, **13**, 2271 (2001).

## Fermi Surface and Electrical Transport Properties of a $\tau$ Phase Organic Conductor

Storr, K., NHMFL

Balicas, L., NHMFL

Brooks, J.S., NHMFL

Graf, D., NHMFL

Papavassiliou, G.C., Theoretical and Physical Chemistry Institute, Greece

We have performed a systematic electrical transport study<sup>1</sup> of the 2-dimensional organic conductor<sup>2</sup>  $\tau$ -P - S, S -DMEDT-TTF $_2$  AuBr $_2$  (AuBr $_2$ ) $_y$  (where  $y\approx 0.75$ ) at low temperatures and high magnetic fields. Both the in-plane and the inter-plane resistivities show a pronounced negative and hysteretic magnetoresistance, which in some samples are followed by the observation of Shubnikov de Haas (SdH) oscillations. Two fundamental frequencies,  $F_{\text{low}}$  and  $F_{\text{high}}$ , are detected in the Fourier transform of

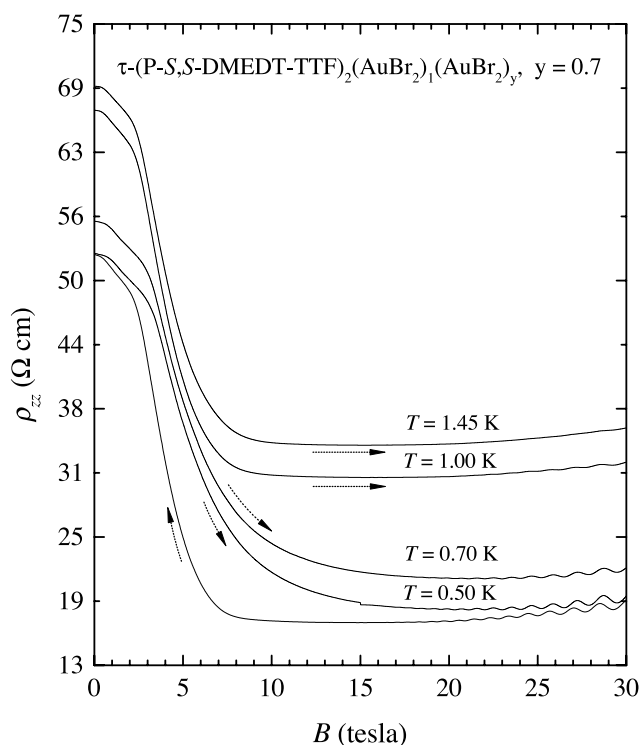


**Figure 1.** Inter-plane resistivity  $\rho_{zz}$  as a function of  $B$  (perpendicular to the conducting layers for different temperatures: 1.45, 1.0, 0.7, and 0.55 K respectively). All curves are vertically displaced for clarity. Arrows indicate field-up and field-down sweeps. The observation of the quantum oscillations at high magnetic fields implies a well-defined metallic state with a Fermi surface.

the SdH signal, corresponding respectively to 2.4% and 6.8% of the area of the first Brillouin zone ( $A_{BZ}$ ). These findings are at odds with band structure calculations, according to which the Fermi surface (FS) is composed of a single star-shaped sheet with an area of 12.5 % of  $A_{BZ}$ . High effective masses,  $\mu_{low}=4.0\pm0.5$  and  $\mu_{high}=7.3\pm0.1$ , were obtained for frequencies  $F_{low}$  and  $F_{high}$  respectively. The angular dependence of  $F_{low}$  and  $F_{high}$  reveal the 2-dimensional character of the FS, while the absence of frequency beatings indicates the absence of warping along the  $k_z$  direction. Furthermore, the angle dependent magnetoresistance (AMRO) suggests a FS which is strictly 2-D, i.e., the inter-plane hopping  $t_c$  is virtually absent or incoherent. While the Hall constant  $R_{xy}$  is field independent, the Hall mobility  $m_H$  increases by a factor of 3, under moderate magnetic fields, which indicates that magnetic field does not change the carrier concentration, but instead, decreases the carriers scattering rate  $\tau$ .

**Acknowledgements:** We are indebted to V. Dobrosavljevic and K. Murata for helpful discussions and S. McCall for his help with the SQUID measurements. We also acknowledge support from NSF-DMR 95-10427 and 99-71474 (JSB). One of us (LB) is grateful to the NHMFL for sabbatical leave support. The NHMFL is supported through a cooperative agreement between the State of Florida and the NSF through NSF-DMR-95-27035.

<sup>1</sup> Storr, K., *et al*, cond-mat/0011529.

<sup>2</sup> Papavassiliou, G.C., *et al.*, *Synth. Met.*, **103**, 1921-1925 (1999); Papavassiliou, G.C., *et al.*, *Synth. Met.*, **86**, 2043-2047 (1997).

## Evolution of Two Positive Components of Magnetoresistance in the Aging Process of FeCl<sub>4</sub>-Doped Polyacetylene ▀IHRP▀

Suh, D.-S., Seoul National Univ., Physics, Korea  
Kim, T.J., Seoul National Univ., Physics, Korea  
Park, Y. W., Seoul National Univ., Physics, Korea,  
and NHMFL

Piao, G., Univ. of Tsukuba, Inst. of Materials  
Science, Japan

Akagi, K., Univ. of Tsukuba, Inst. of Materials  
Science, Japan

Shirakawa, H., Univ. of Tsukuba, Inst. of Materials  
Science, Japan

Brooks, J.S., NHMFL/FSU, Physics

Magnetotransport of heavily doped polyacetylene has been investigated to understand its intrinsic metallic conduction properties at low temperatures. It is well known that the negative magnetoresistance of a fresh sample changes to be positive as the sample ages. The characteristic of the change from the negative to the positive magnetoresistance in the aging process is dependent on the type of dopants, and this difference was studied previously in the low magnetic field region.<sup>1</sup> Here, we present the high field magnetoresistance of FeCl<sub>4</sub>-doped high-density polyacetylene films in different aging levels at  $T=0.6\sim1.4$  K and  $H=0\sim30$  T, which has not been explored yet.

Fig. 1 shows the temperature dependence of the resistivity and the magnetoresistance of  $\text{FeCl}_4^-$ -doped high-density polyacetylene films. In Fig. 1 (a), (b), and (c), the sample A1 is fresh and the sample A2 is aged. For A1, with  $\sigma(300\text{K})=12000$  S/cm, the zero-field temperature dependence of resistivity shows a resistivity minimum at around  $T=200$  K. In Fig. 1 (b), the sample A1 shows negative magnetoresistance up to  $H=30$  T. For the aged sample, A2 with  $\sigma(300\text{K})=6000$  S/cm, the magnetoresistance up to  $H=30$  T is negative except at very low fields, but the magnitude of negative magnetoresistance is much larger than that of the sample A1 and the field dependence of magnetoresistance of the sample A2 starts to deviate from the linear behavior at two field regions, one at around  $H=2$  T and the other at around  $H=10$  T, as plotted in Fig. 1 (c). For another sample named B1 (fresh) and B2 (aged), the data are plotted in Fig. 1 (d), (e), and (f). The sample B1 with  $\sigma(300\text{K})=18000$  S/cm shows the negative magnetoresistance as in Fig. 1 (e). The change of the magnetoresistance with respect to the degree of aging is much more clearly observed for the sample B2 with  $\sigma(300\text{K})=4000$  S/cm. In Fig. 1 (f), two positive components of magnetoresistance appear. The first one forms the sharp peak around  $H=2\sim 3$  T and the second one evolves with a broad peak around  $H=15$  T at  $T=0.60$  K. As temperature increases from  $T=0.60$  K to  $T=1.41$  K, the magnitude of the low field positive peak decreases and the second positive peak in the high field region moves slightly to a higher field region.

Compared to the iodine-doped aged polyacetylene films with the magnetoresistance of single positive broad peak, the  $\text{FeCl}_4^-$ -doped aged polyacetylene films show completely different behaviors as described above. The larger normalized resistivity,  $\rho_r(T)=\rho(T)/\rho(300\text{K})$ , and the nonmonotonic magnetoresistance behavior observed in aged  $\text{FeCl}_4^-$ -doped polyacetylene in high magnetic fields are thought to be originated from the subtle interplay of several mechanisms. One of the approaches to explain the obtained results is as follows. For the low field positive magnetoresistance, the effect of the spin-dependent variable-range-hopping conduction was discussed in another publication.<sup>1</sup> It argued the energy distance

between the mobility edge and the Fermi energy ( $\Delta E=E_C-E_F=2\sim 3\text{meV}$ ) was small for  $\text{FeCl}_4^-$ -doped aged polyacetylene films, but larger energy distance ( $\Delta E>10\text{meV}$ ) for iodine-doped aged films. We suggest that the electrical transport of the disordered system can be related in particular to a significant spatial inhomogeneity, which especially results in the spatial dependence of the mobility edge  $E_C$ . Consequently, the energy distance ( $\Delta E=E_C-E_F$ ) spreads over the energy scale from several meV down to zero in different positions. In this  $\text{FeCl}_4^-$ -doped aged polyacetylene films, the field dependence of magnetoresistance becomes complicated because of the small energy distance ( $\Delta E=E_C-E_F$ ), which is strongly affected by the change of the mobility edge under high magnetic fields and consequently gives the second positive component of magnetoresistance in the high field region.

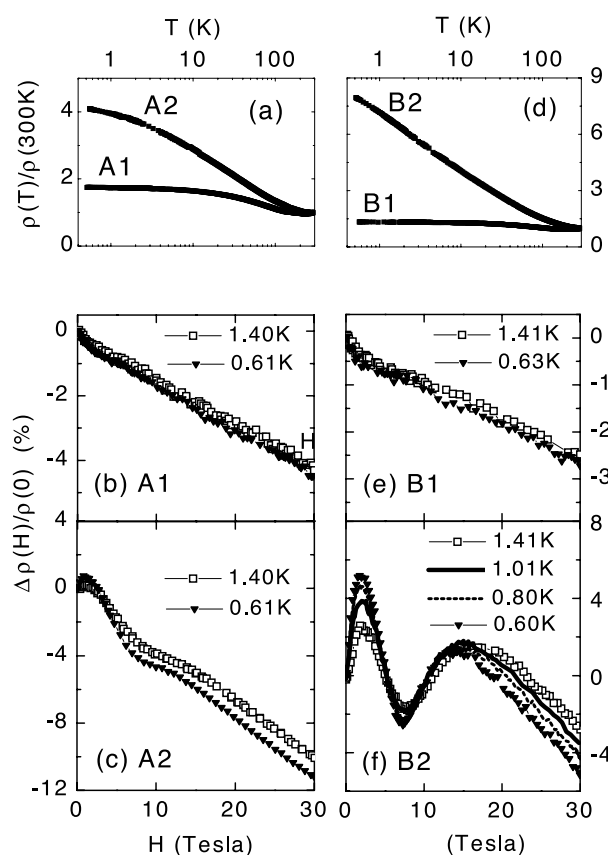


**Figure 1.** (a), (d) Temperature dependence of the normalized resistivity and (b), (c), (e), (f) the magnetoresistance of the stretch-oriented high-density polyacetylene films heavily doped with  $\text{FeCl}_4^-$ . A1 (B1) and A2 (B2) are the identical samples with different aging level.



**Acknowledgements:** This research was supported by KISTEP with 98-I-01-04-A-026. The NHMFL is supported through a Cooperative Agreement between the NSF through NSF-DMR-95-27035 and the State of Florida.

<sup>1</sup> Kaneko, H., *et al.*, Solid State Commun., **90**, 83-87 (1994).

## High Field Magnetoconductivity of Iodine-Doped Helical Polyacetylene

■ IHRP ■

Suh, D.-S., Seoul National Univ., Physics, Korea  
Kim, T.J., Seoul National Univ., Physics, Korea  
Park, Y.W., Seoul National Univ., Physics, Korea  
and NHMFL

Piao, G., Univ. of Tsukuba, Inst. of Materials  
Science, Japan

Akagi, K., Univ. of Tsukuba, Inst. of Materials  
Science, Japan

Shirakawa, H., Univ. of Tsukuba, Inst. of Materials  
Science, Japan

Brooks, J.S., NHMFL/FSU, Physics

Because of the interesting morphology of helical polyacetylene consisting of twisted fibers,<sup>1</sup> the effect of the magnetic field on the subject compound has been investigated to examine the intrafibrillar and the interfibrillar interaction in the electrical conduction process of the polymeric system. For this purpose, we measured the magnetoconductivity of the R-type helical polyacetylene heavily doped with iodine in the range of  $T = 0.60\text{ K} \sim 1.40\text{ K}$  and  $H = 0\text{ T} \sim 30\text{ T}$ . The characteristic behaviors at low fields and at high fields show that the three-dimensional (anisotropic) weak localization theory, which is usually applied in the case of doped high-density polyacetylene, is not appropriate to explain the field dependence of the conductivity of the doped helical polyacetylene.

The R-type helical polyacetylene was doped with iodine in the gas phase up to the saturation level ( $\sim 10$  molar%), right before the transport measurement. The room temperature conductivity was  $\sigma(300\text{ K}) \approx 100\text{ S/cm}$ . Such a low room temperature conductivity is due to its low density

property. All the experiment processes, including the doping and the magnetoconductivity measurement up to  $H = 30\text{ T}$ , were performed at the NHMFL in Tallahassee. The temperature dependence of resistivity and the (longitudinal) magnetoconductivity are plotted in Fig. 1 (a) and (b). The zero-field resistivity ratio was  $\rho(0.5\text{ K})/\rho(300\text{ K}) = 30$ ; the temperature dependence was logarithmic in the low temperature range; and the magnetoconductivity was negative at low fields, but became positive in the high field region. (Magnetoresistance was positive at low fields and negative at high.)

For the high field positive magnetoconductivity up to  $H = 30\text{ T}$ , the obtained data clearly show the linear  $H$  dependence, and they are almost insensitive to the temperature. The origin of this linear dependence is under consideration. However, it is clear that the

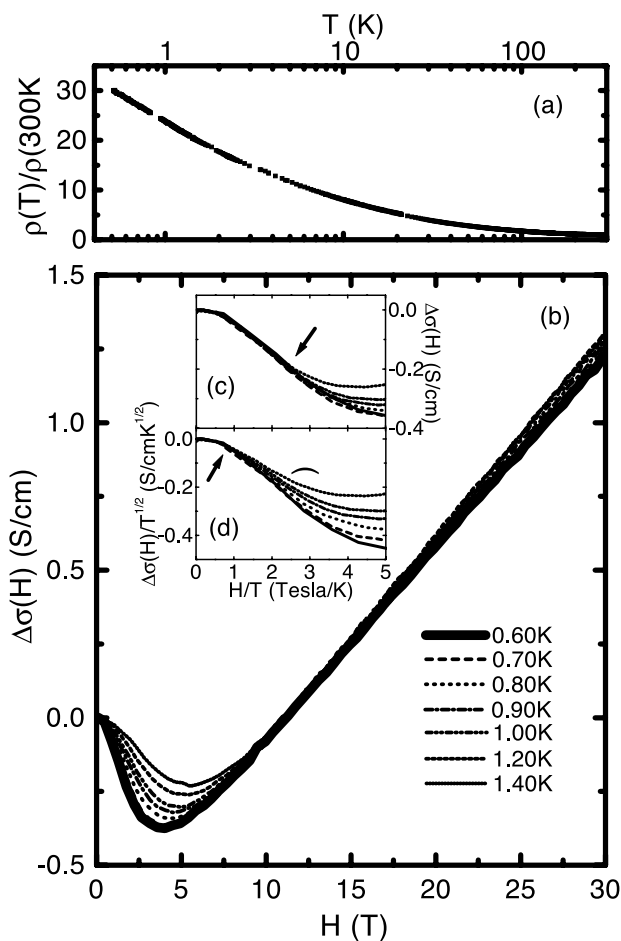


**Figure 1.** (a) The temperature dependence of resistivity and (b) the magnetoconductivity of iodine-doped helical polyacetylene. The low  $H/T$  data are plotted in the scheme of (c)  $\Delta\sigma(H,T)$  vs.  $H/T$  and (d)  $\Delta\sigma(H,T)/T^{1/2}$  vs.  $H/T$  in inset figures.



three-dimensional localization-interaction picture, which is usually applied to the doped high-density polyacetylene, is insufficient to explain this linear  $H$  dependence because that theory predicts the  $H^{1/2}$  dependence of the magnetoconductivity.

To examine the field dependence of the low field negative magnetoconductivity (i.e. positive magnetoresistance), we replotted our data in the scheme of (c)  $\Delta\sigma$  versus  $H/T$  and (d)  $\Delta\sigma/T^{1/2}$  versus  $H/T$ . In Fig. 1 (c), all the data follow the same line up to  $H/T \sim 2.4$ , but in Fig. 1 (d), they start to deviate from each other at  $H/T \sim 1$ . If the negative magnetoconductivity originates from the electron-electron interaction in a three-dimensional disordered metallic system, the data of the inset (b) (showing  $\Delta\sigma(H)/T^{1/2}$  versus  $H/T$  plot) are expected to follow one single curve. However, the data of Fig. 1 (c) (with the  $\Delta\sigma$  versus  $H/T$  plot) follow one single curve up to the higher  $H/T$  value than the data in Fig. 1 (d) as pointed by the arrow in the figure. This indicates that  $H/T$  is the single parameter determining  $\Delta\sigma(T,H)$  in the low  $H/T$  region, i.e.,  $\Delta\sigma(T,H) = f(H/T)$ .

**Acknowledgements:** This research was supported by KISTEP with 98-I-01-04-A-026. The NHMFL is supported through a Cooperative Agreement between the NSF through NSF-DMR-95-27035 and the State of Florida.

<sup>1</sup> Akagi, K., *et al.*, Science, **282**, 1683-1686 (1998).

## A New Damping Mechanism in the Angle Dependence of Magnetic Quantum Oscillations in Quasi-Two-Dimensional Organic Metals

Symington, J.A., Univ. of Oxford, Physics

Singleton, J., Univ. of Oxford, Physics

Schrama, J.M., Univ. of Oxford, Physics

Ardavan, A., Univ. of Oxford, Physics

Harrison, N., LANL

Kurmoo, M., IPCMS, France

Day, P., The Royal Institution, London

Schlueter, J., Argonne National Laboratory

We have carried out detailed magnetic-field-orientation dependent studies of the magnetic quantum oscillations in a number of quasi-two-dimensional (Q2D) organic molecular metals. Previously, we and others have noted that separate neck and belly orbits are not observed about the Fermi surfaces of such systems, even though the Fermi surfaces are expected to be warped Q2D cylinders.<sup>1,2</sup> This observation implies that the low-field quantum oscillations in such systems should be treatable using the two-dimensional form of the Lifshitz-Kosevich formalism.<sup>2</sup> It is, therefore, possible to predict the precise angle dependence that the oscillations should follow.

In Fig. 1, we show the theoretical prediction compared with typical experimental data.<sup>1</sup> Note that the experimental oscillation amplitudes are attenuated more rapidly with increasing tilt angle  $\theta$  than the theoretical prediction suggests that they should be; here,  $\theta$  is the angle between the normal to the Q2D planes and the magnetic field. Detailed study shows that the additional attenuation can be represented accurately as  $\exp(-a \tan \theta)$ , where  $a$  is a constant which depends on the material studied. This behavior seems to occur UNIVERSALLY in the (BEDT-TTF) charge-transfer salts that we have studied thus far, independent of the exact details of the crystal structure (a  $\beta$ -phase salt,  $\beta''$ -phase salt, and two  $\alpha$ -phase salts have been measured). Moreover, the attenuation affects both de Haas-van Alphen and Shubnikov-de Haas oscillations.

We have derived a model that is able to account fully for these observations.<sup>1</sup> The model considers the variation of the density of states for scattering at the Fermi surface with  $k_z$ , the component of  $k$  in the interplane direction. Fig. 2 shows a plot of contours representing the scattering rate plotted on a warped cylindrical Fermi surface. The scattering rate is small on the torso of the Fermi surface, but large on the neck and bellies, thereby suppressing the separate neck and belly oscillations. On tilting the field, the orbits of more and more quasiparticles intersect the bands on the necks and bellies that correspond to

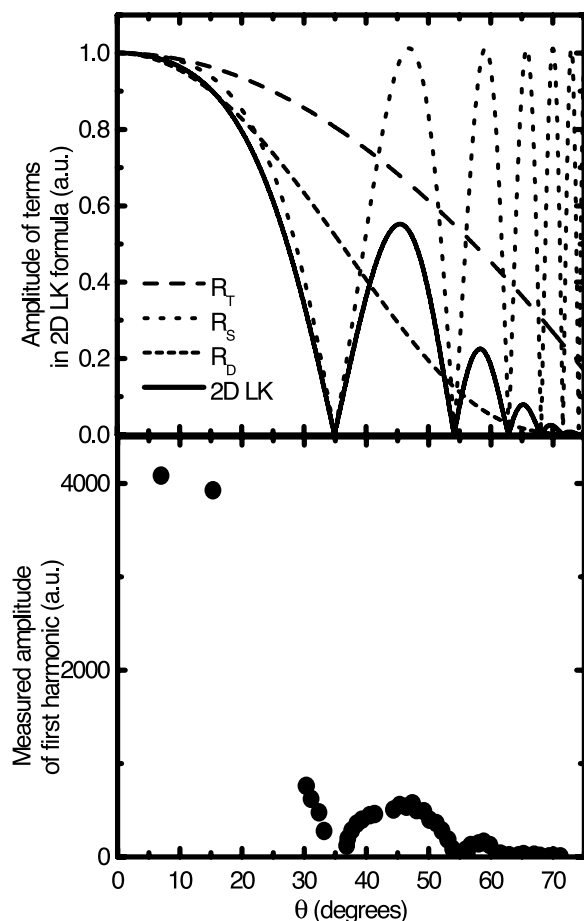


**Figure 1.** Top: theoretical prediction of the angle dependence of the amplitude of magnetic quantum oscillations in  $\beta''$ -(BEDT-TTF)<sub>2</sub>SF<sub>5</sub>CH<sub>2</sub>CF<sub>2</sub>SO<sub>3</sub>. The dotted lines are the various phase-smearing terms from the Lifshitz-Kosevich theory;  $R_T$  thermal term;  $R_D$  damping term due to scattering;  $R_S$  oscillatory term due to spin-splitting. The solid line is the overall expected angle dependence, and is a convolution of the three phase-smearing terms. Bottom: experimental data (points) from  $\beta''$ -(BEDT-TTF)<sub>2</sub>SF<sub>5</sub>CH<sub>2</sub>CF<sub>2</sub>SO<sub>3</sub>. Note how the data decline with increasing angle much more rapidly than predicted by theory.

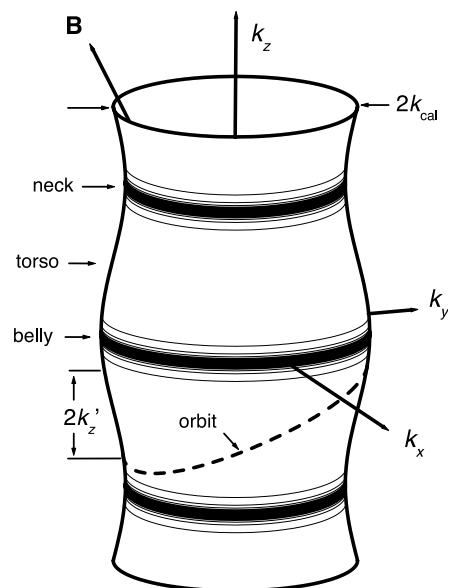


**Figure 2.** Scattering rate contours on a warped cylindrical Fermi surface (low scattering rate on the torso; high rates on the neck and belly). A cyclotron orbit (always in the plane perpendicular to the magnetic field) is shown. As the tilt angle grows, the orbit will intersect more and more of the areas where scattering is rapid.

large scattering rates, thus attenuating the quantum oscillations.

Taken in conjunction with millimetre-wave experiments done at NHMFL,<sup>3,4</sup> these studies provide compelling evidence that the interplane transport in organics is coherent.

<sup>1</sup> Symington, J.A., *et al.*, Synth Met., in press; Phys. Rev. Lett., to be submitted.

<sup>2</sup> Singleton, J., Reports on Progress in Physics, **63**, 1111 (2000).

<sup>3</sup> Edwards, R.S., *et al.*, Synth Metals, in press; Phys. Rev. Lett., submitted.

<sup>4</sup> Schrama, J.M., *et al.*, J. Phys.: Condens. Matter, **13**, 2235 (2001).

# Thermal Activation Between Landau Levels in the Organic Superconductor $\beta''$ -(BEDT-TTF)<sub>2</sub>SF<sub>5</sub>CH<sub>2</sub>CF<sub>2</sub>SO<sub>3</sub>

Symington, J.A., Univ. Of Oxford, Physics  
 Singleton, J., LANL  
 Nam, M.-S., Univ. Of Oxford, Physics  
 Harrison, N., LANL  
 Mielke, C.H., LANL  
 Schlueter, J.A., Argonne National Laboratory  
 Williams, J.M., ANL

We have performed measurements of quantum oscillations in the quasi-two-dimensional organic superconductor  $\beta''$ -(BEDT-TTF)<sub>2</sub>SF<sub>5</sub>CH<sub>2</sub>CF<sub>2</sub>SO<sub>3</sub> in fields of up to 60 T provided by NHMFL/LANL.<sup>1</sup> Fig. 1 shows the temperature dependence of the interplane magnetoresistance, which exhibits very pronounced Shubnikov-de Haas (SdH) oscillations. The SdH frequency is in good agreement with recent angle-dependent magnetoresistance oscillation (AMRO) measurements in this material.<sup>2,3</sup>

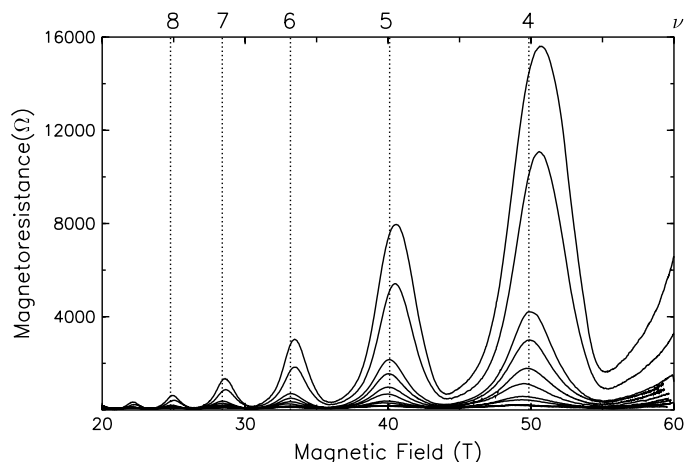


**Figure 1.** Temperature dependence of the interplane magnetoresistance of  $\beta''$ -(BEDT-TTF)<sub>2</sub>SF<sub>5</sub>CH<sub>2</sub>CF<sub>2</sub>SO<sub>3</sub>. (From the top,  $T = 0.59, 0.94, 1.48, 1.58, 1.91, 2.18, 2.68, 3.03, 3.38, 3.80$ , and  $4.00$  K). The dotted lines and numbers indicate integer Landau-level filling factors.

At values close to integer Landau-level filling factors,  $\nu = F/B$ , the sample resistance becomes very large at low temperatures  $T$ . Fig. 2 shows the resistance at these peak values plotted as  $\log \sigma$  (where  $\sigma \propto 1/(\text{sample resistance})$ ) versus  $1/T$ . For a significant

range of temperature, the conductivity  $\sigma$  shows activated behavior.<sup>1</sup> The inset to Fig. 2 shows the energy gap  $E_g$  deduced from the activated behavior plotted as a function of magnetic field alongside the function  $\hbar\omega_c - E_0$  (solid line). With  $E_0$  set to  $1.23$  meV, the experimental values of  $E_g$  all lie close to this line, strongly supporting the proposal that  $E_g$  is related to the gap between the Landau-level centres  $\hbar\omega_c$ .<sup>1</sup> Landau-level broadening will cause a reduction of the effective energy gap, and it is this reduction that we identify with  $E_0$ , which is about three times the Landau-level half-width of  $0.44$  meV deduced from the Dingle temperature.<sup>1</sup>

In summary, we have observed thermally-activated conductivity at integer Landau-level filling factors. To our knowledge, this is the first identification of such a mechanism in a metallic system. The

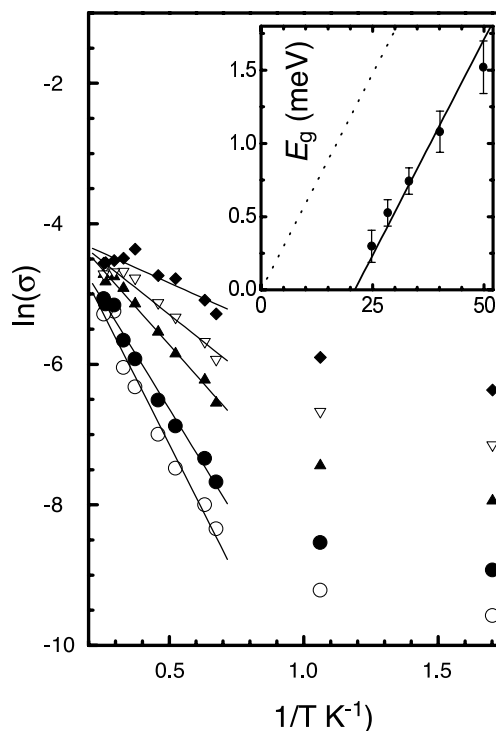


**Figure 2.**  $\log \sigma$  (where  $\sigma \propto 1/(\text{sample resistance})$ ) versus  $1/T$  at the magnetoresistance peaks close to integer filling factors; filled diamond  $F/B = 8$ , open triangle  $F/B = 7$ , filled triangle  $F/B = 6$ , filled circle  $F/B = 5$ , and open circle  $F/B = 4$ . The lines are fits used to extract the energy gaps. The inset shows the energy gap  $E_g$  deduced from the activated behavior plotted as a function of magnetic field alongside the function  $\hbar\omega_c - E_0$  (solid line). The dotted line shows  $\hbar\omega_c$  for comparison.

activation energies deduced from the conductivity are in good agreement with the Landau-level spacings once broadening is taken into account suggesting that the recent identification of a “field-induced insulator” in this material is incorrect.<sup>4</sup> To account for this behavior and for magnetization<sup>5</sup> and resistivity<sup>2,4</sup> data, we propose that the Q1D sheets of the Fermi surface of  $\beta''$ -(BEDT-TTF)<sub>2</sub>SF<sub>5</sub>CH<sub>2</sub>CF<sub>2</sub>SO<sub>3</sub> are nested.<sup>1</sup> The temperature dependence of the resistivity suggests that this occurs at about 140 K.<sup>1</sup>

<sup>1</sup> Nam, M.S., *et al.*, submitted to Phys. Rev. Lett.

<sup>2</sup> Edwards, R., *et al.*, submitted to Phys. Rev. Lett.

<sup>3</sup> Beckmann, D., *et al.*, Eur. Phys. J. B, **1**, 295 (1998).

<sup>4</sup> Wosnitza J., *et al.*, Phys. Rev. B, **61**, 7383 (2000).

<sup>5</sup> Wosnitza, J., *et al.*, preprint cond-mat-0011357 21 Nov. 2000.

## Unusual High-Field Transport Properties of the Two-Dimensional Organic Metal $\kappa$ -(BEDT-TTF)<sub>2</sub>I<sub>3</sub>

Wosnitza, J., Physikalisches Institut, Universität Karlsruhe, Germany

Harrison, N., NHMFL/LANL

Balicas, L., NHMFL/FSU, Physics

Brooks, J.S., NHMFL/FSU, Physics

Schweitzer, D., 3. Physikalisches Institut, Universität Stuttgart, Germany

The pronounced two-dimensional (2D) electronic structure of organic metals of the type (BEDT-TTF)<sub>2</sub>X is reflected in a variety of extraordinary electronic features. At sufficiently high fields and low temperatures, the 2D metals  $\alpha$ -(BEDT-TTF)<sub>2</sub>KHg(SCN)<sub>4</sub> and  $\kappa$ -(BEDT-TTF)<sub>2</sub>I<sub>3</sub>, for instance, can no longer be described by the conventional 3D theory for magnetic quantum oscillations. In addition, these metals reveal strong eddy-current resonances in pulsed magnetic fields. The latter is most probably caused by exceptionally high in-plane conductivities, which, at least for  $\alpha$ -(BEDT-TTF)<sub>2</sub>KHg(SCN)<sub>4</sub>, seem to be connected with features resembling the behavior of a type-II superconductor, i.e., at certain high-field values the resistivity decreases rapidly with decreasing temperature and a hysteretic behavior of the

magnetization appears.<sup>1</sup> Consequently, one goal of the present investigation was the search for a corresponding effect in  $\kappa$ -(BEDT-TTF)<sub>2</sub>I<sub>3</sub>. Since for this material the eddy-current resonances appeared only above about 30 T,<sup>2</sup> steady fields in a higher range are necessary, which up to now are only available with the hybrid magnet at Tallahassee.

In our experiment, we succeeded in measuring simultaneously the interplane resistance and the magnetization,  $M$ , of one  $\kappa$ -(BEDT-TTF)<sub>2</sub>I<sub>3</sub> single crystal by use of a capacitive cantilever torque magnetometer. Fig. 1 shows the well-resolved quantum oscillations in both signals. The inset shows the absence of any kind of hysteresis for data taken at rising (diamonds) and falling (solid line) field. This either means that still higher fields are necessary to resolve a hysteresis in  $M$  or it reflects a different origin of the eddy-current resonances for the two 2D metals.

The simultaneous measurement of both transport and magnetization data allowed us to directly study the field and temperature dependent evolution of the difference between Shubnikov-de Haas (SdH) and de Haas-van Alphen (dHvA) oscillations. At moderately high fields of about 15.7 T, the SdH signal, i.e., the relative conductivity oscillations, is very similar to the derivative of the dHvA signal times the field squared, i.e., proportional to

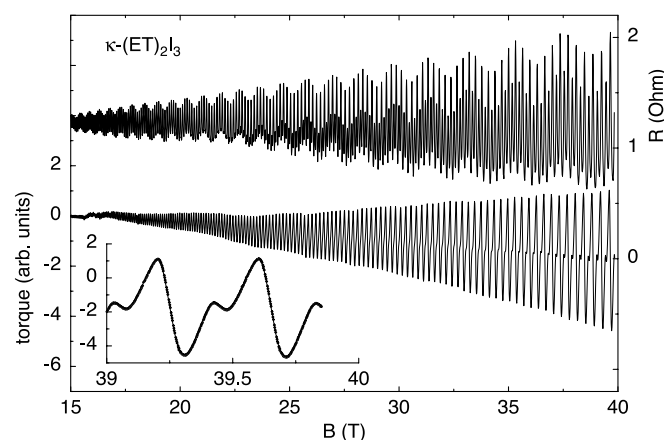


**Figure 1.** Simultaneously measured resistance (upper trace) and torque (lower trace) acting on a  $\kappa$ -(BEDT-TTF)<sub>2</sub>I<sub>3</sub> sample. The inset shows the absence of any hysteresis in the up (diamonds) and down sweep (solid line).

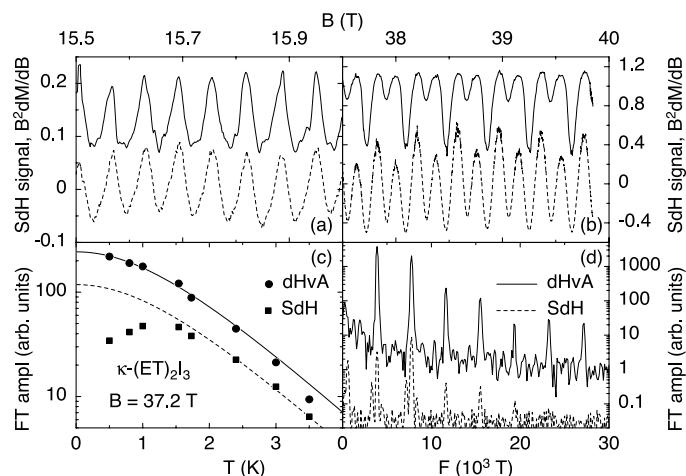


**Figure 2.** Comparison of the SdH signal with  $B^2 dM/dB$  extracted from the torque data at lower (a) and higher (b) fields. (c) The temperature dependence of the oscillation amplitude at about 3870 T from dHvA and SdH data with effective-mass fits for  $m_c = 3.8 m_e$ . (d) The Fourier transformations of the high-field ( $30 \text{ T} < B < 40 \text{ T}$ ) dHvA and SdH data.

$B^2 dM/dB$  (Fig. 2a), as theoretically expected. Towards higher fields, however, the SdH signal reveals a much stronger second harmonic than the dHvA signal (Fig. 2b), seen also from the Fourier transformations of both signals (Fig. 2d). Obviously, the SdH signal gets damped at high magnetic fields; this becomes especially apparent in a strongly reduced fundamental SdH oscillation amplitude towards lower temperatures (Fig. 2c) and higher fields (not shown).<sup>3</sup> Consequently, the effective masses and the Dingle temperatures cannot be extracted from the transport data in a reliable way. Our result clearly shows that the conventional theory for the appearance of magnetic quantum oscillations in the resistivity is no longer valid for  $\kappa-(\text{BEDT-TTF})_2\text{I}_3$  at high fields.

<sup>1</sup> Harrison, N., *et al.*, Phys. Rev. B, **62**, 14 212 (2000).

<sup>2</sup> Harrison, N., *et al.*, Phys. Rev. B, **58**, 10248 (1998).

<sup>3</sup> Wosnitza, J., *et al.*, Physica B, in press.

## Upper Critical Field Studies in Organic Superconductor $\kappa-(\text{BEDT-TTF})_2\text{Cu}(\text{SCN})_2$

Zuo, F., Univ. of Miami, Physics

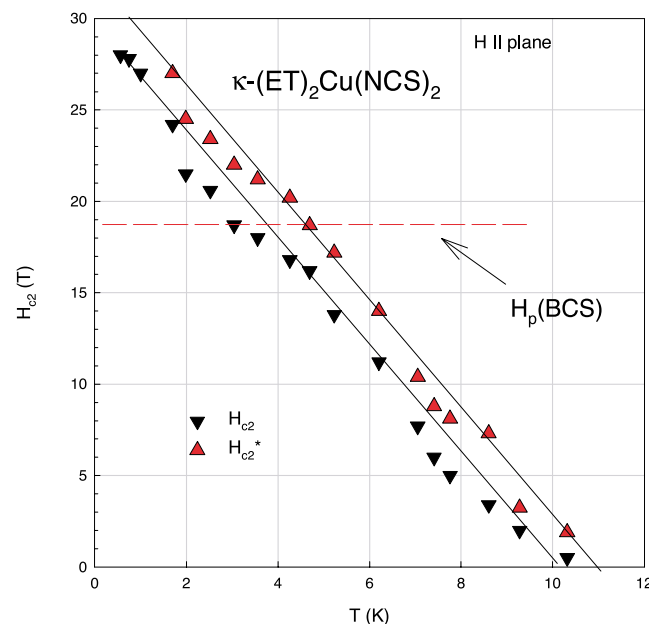
Brooks, J.S., NHMFL/FSU, Physics

McKenzie, R.H., Univ. of New South Wales, Physics

Schlueter, J.A., Argonne National Laboratory

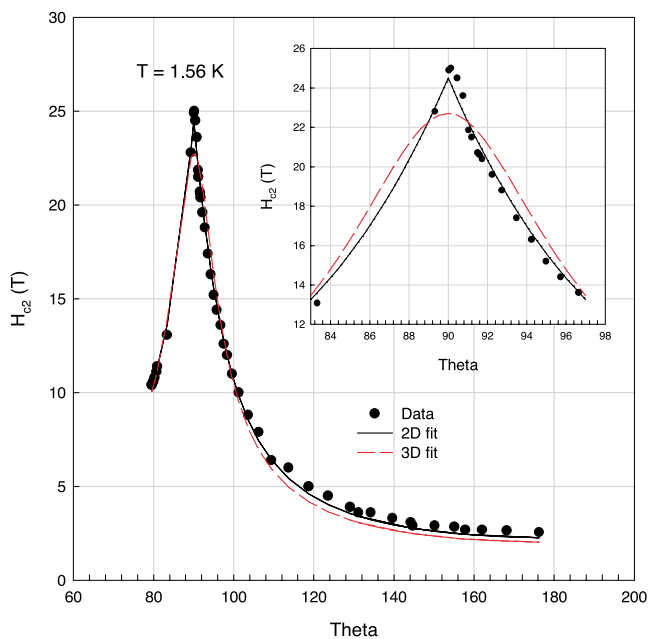
We have carried out extensive magnetotransport measurements on the organic superconductor  $\kappa-(\text{BEDT-TTF})_2\text{Cu}(\text{SCN})_2$ , for temperature down to 0.5 K and field up to 30 T. For field parallel to the plane direction, the upper critical field determined resistively exceeds considerably the BCS Pauli paramagnetic limit.<sup>1</sup>

Fig. 1 is a plot of the temperature dependence of the upper critical field for the parallel direction. The upper critical field at  $T=0$  K limit is about 30 T. This is much larger than the 18 T expected from the BCS limit. The two values for the upper critical field are obtained using different criteria.<sup>1</sup> Both values show quasi-linear with temperature.



**Figure 1.** Temperature dependence of the upper critical field in the parallel direction.





**Figure 2.** Angular dependence of the upper critical field. The inset shows the expanded view about the parallel direction.

Shown in Fig. 2 is a direct plot of the angular dependence of the upper critical field. The lines are fit to the 2D and 3D models. The inset shows the expanded view around the parallel direction, with the solid line as a fitting to the 2D model and dashed line fit to the 3D model. Clearly, the 2D model fits much better than the 3D, an isotropic model.

The origin of the large upper critical field is not clear. It has been suggested that the upper critical field and its angular dependence may be consistent with the existence of inhomogeneous superconductivity. Further experimental characterizations on other layered organic superconductors are necessary.

<sup>1</sup> Zuo, F., *et al.*, Physical Review B, **61**, 750 (2000).